



Strål
säkerhets
myndigheten

Swedish Radiation Safety Authority

Research

Alpha spectrometry of radioactive aerosols from the European Spallation Source

– an investigation of the possibilities of direct
alpha spectrometry.

2024:07

Author: Kristina Eriksson Stenström, Guillaume Pédehontaa-Hiaa,
Belikse Ramljak, Christopher Rääf

Date: April 2024

Report number: 2024:07

ISSN: 2000-0456

Available at www.ssm.se



Strål
säkerhets
myndigheten

Swedish Radiation Safety Authority

Author: Kristina Eriksson Stenström¹, Guillaume Pédehontaa-Hiaa^{1,2}
Belikse Ramljak¹, Christopher Rääf²

¹Department of Physics, Division of Nuclear Physics,
Lund University, Sweden

²Department of Translational Medicine, Medical Radiation Physics,
Malmö, Lund University, Sweden

2024:07

Alpha spectrometry of radioactive aerosols from the European Spallation Source – an investigation of the possibilities of direct alpha spectrometry.

Date: April 2024

Report number: 2024:07

ISSN: 2000-0456

Available at www.stralsakerhetsmyndigheten.se

This report was commissioned by the Swedish Radiation Safety Authority (SSM). The conclusions and viewpoints presented in the report are those of the author(s) and do not necessarily coincide with those of SSM.

SSM perspektiv

Bakgrund

I Lund pågår byggandet av forskningsanläggningen European Spallation Source (ESS) och anläggningen genomgår även ett stegvis tillståndsförfarande i enlighet med relevanta lagkrav. Vid ESS kommer neutroner att produceras genom spallation när högenergi protoner från en linjäraccelerator träffar ett roterande volframstrålemål. Neutronerna som frigörs från strålmålet kommer att användas för olika vetenskapliga experiment.

Strålsäkerhetsmyndigheten (SSM) utlyste 2021 medel till forskning för att utveckla mätmetoder för de specifika radionuklider som kan inträffa vid utsläpp i en händelse utöver förväntad drift från forskningsanläggningen European Spallation Source (ESS) i Lund. Syftet med utlysningen var att möjliggöra vidareutveckling av användbara mätmetoder och särskilt med hänsyn till de specifika radionuklider som har visat sig dominera dosbidraget till allmänheten.

I rapporten Underlag till beredskapsplanering kring ESS (SSM 2018:22) framgår att ^{148}Gd , ^{187}W , ^{172}Hf , ^{182}Ta och $^{178\text{n}}\text{Hf}$ är de radionuklider som bidrar mest till den effektiva dosen till allmänheten vid dimensionerande händelser för beredskapsplanering kring anläggningen. I den dimensioneringshändelse som beskrivs i Strålsäkerhetsmyndighetens rapport SSM2018:02, och som ligger till grund för placering av ESS-anläggningen i hotkategori II, bidrar inhalationsdosen till mer än 50 % av den effektiva dosen under de första 7 dagar efter olyckan. Mer än hälften av den totala effektiva dosen under denna period kommer från ^{148}Gd (halveringstid=71,1 år; E_{α} =3183 keV). Även vid normal drift kan små mängder ^{148}Gd och andra radioaktiva nuklider släppas ut i miljön via stackar kopplade till ESS-anläggningens ventilationssystem. För korrekta dosuppskattningar behövs tekniker för att mäta ^{148}Gd i omgivande prover. Eftersom ^{148}Gd förväntas förekomma i aerosolform och eftersom inhalationsdosen är av största vikt är uppsamling av luftburna aerosoler i luft lämplig.

Denna rapport syftar till att beskriva de grundläggande kraven för att kunna kvantifiera ^{148}Gd i aerosolprover som samlats in från omgivande luft i ESS på filter med hjälp av speciella luftprovtagare, både under normal drift och vid ett olycksscenario. Fokus ligger på att utvärdera möjligheten för direkt alfaspektrometri, där alfastrålningen från filterprovet mäts utan förbehandling.

Resultat

Analysen av filtren visar att det mesta av alfaaktiviteten från radondöttrar på filtren har försvunnit efter några dagar. En uppskattning av det tjockaste lämpliga aerosolskiktet presenteras, samt förslag på lämpliga luftflöden och uppsamlingstider som kan möjliggöra direkt alfaspektrometri av aerosolprover insamlade på filter för miljöövervakningsändamål och som nödberedskap vid oavsiktliga utsläpp. Energiupplösningen kommer inte bara att bero på tjockleken på aerosolskiktet, utan också på storleken på aerosolpartiklarna och i vilken utsträckning de penetrerar filtret. Bästa energiupplösning erhålls för tunna skikt (< 200 $\mu\text{g cm}^{-2}$), små partiklar (<<1 μm i diameter) och obefintlig penetration i filtret. Låga insamlingsflöden är därför nödvändiga.-

Relevans

Kunskaper om mätmetoder och deras tillämpning för de specifika radionuklider som produceras vid ESS är av stort intresse då det ökar möjligheten att ta fram bättre data vid händelser utöver förväntad drift. Denna kunskap kan också vara användbar för operatören och andra liknande anläggningar i världen. Denna forskning är också ett bidrag till att stärka den nationella kompetensen inom strålsäkerhet, vilket ligger i linje med de behov som identifierats i regeringsuppdraget "Grunden för en långsiktig kompetensförsörjning inom strålsäkerhetsområdet" (SSM2017-134-23). SSM avser att använda resultaten i så stor utsträckning som möjligt inom tillståndsprövning och tillsyn och sprida informationen till myndigheter som reglerar liknande verksamhet.

Behov av vidare forskning

Eftersom dosimetri av radioaktiva aerosoler hos människa är nära kopplad till storleken på aerosolpartiklarna, rekommenderas att ytterligare undersöka möjligheten till direkt alfaspektrometri efter insamling med system som fraktionerar aerosolerna efter storlek (impactor systems). Störningarna i alfaspektra från andra typer av strålning behöver undersökas ytterligare (t.ex. sammanträffanden mellan alfa och andra typer av joniserande strålning, eller påverkan av andra typer av joniserande strålning som registreras i alfadetektorn). Ytterligare uppskattningar av den förväntade storleken på ^{148}Gd -innehållande aerosoler som genereras vid olika förhållanden vid ESS behövs också för att utvärdera potentialen för direkt alfaspektrometri.

Projektinformation

Kontaktperson SSM: **Karin Aquilonius**

Referens: SSM2021-787/ 4530523

SSM perspective

Background

In Lund, the construction of the European Spallation Source (ESS) research facility is underway and the facility is also undergoing a stepwise licensing procedure in accordance with relevant legal requirements. At ESS, neutrons will be produced by spallation when high-energy protons from a linear accelerator hit a rotating tungsten beam target. The neutrons released from the radiation target will be used for various scientific experiments.

The Radiation Safety Authority (SSM) announced in 2021 funds for research to develop measurement methods for the specific radionuclides that may occur in the event of a release in an event beyond expected operation from the research facility European Spallation Source (ESS) in Lund. The purpose of the call was to enable further development of useful measurement methods and especially with regard to the specific radionuclides that have been shown to dominate the dose contribution to the public.

In the report *Underlag till beredskapsplanering kring ESS* (SSM 2018:22) it appears that ^{148}Gd , ^{187}W , ^{172}Hf , ^{182}Ta and $^{178\text{n}}\text{Hf}$ are the radionuclides that contribute the most to the effective dose to the public in the event that considered as dimensioning for emergency planning around the facility. In the dimensioning event described in the Swedish Radiation Safety Authority's report SSM2018:02, and which is the basis for placement of the ESS facility in threat category II, the inhalation dose is attributed to more than 50% of the effective dose during the first 7 days after the accident. More than half of the total effective dose during this period originates from ^{148}Gd (half-life=71.1 y; E_{α} =3183 keV). Even during normal operation, small amounts of ^{148}Gd and other radioactive nuclides may be released into the environment via stacks connected to the ESS facility's ventilation system. For correct dose estimates, techniques to measure ^{148}Gd in ambient samples are needed. Since ^{148}Gd is expected to appear in aerosol form and since the inhalation dose is of the greatest importance, collection of airborne aerosols in air is suitable.

The present report aims to describe the basic requirements for being able to quantify ^{148}Gd in aerosol samples collected from ambient air of the ESS on filters using special air samplers, both during normal operation and at an accident scenario. The focus is on evaluating the possibility of direct alpha spectrometry, where the alpha radiation from the filter sample is measured without pre-treatment.

Results

The analysis of the filters shows that most of the alpha activity from the radon progenies on the filters has vanished after a few days. An estimate of the thickest suitable aerosol layer is presented, as well as suggestions for suitable airflows and collection times that may enable direct alpha spectrometry of aerosol samples collected on filters for environmental monitoring purposes and as emergency preparedness in case of accidental releases. The energy resolution will not only depend on the thickness of the aerosol layer, but also on the size of the aerosol particles and the extent to which they penetrate the filter. Best energy resolution is obtained for thin layers ($< 200 \mu\text{g cm}^{-2}$), small particles ($\ll 1 \mu\text{m}$ in diameter) and non-existent penetration in the filter. Low collection flows are therefore necessary.

Relevance

Knowledge of measurement methods and their application for the specific radionuclides produced at ESS is of vital interest as it increases the possibility of producing better data in the event of events beyond expected operation. This knowledge can also be useful for the operator and other similar activities in the world. This research is also a contribution to strengthening the national competence in radiation safety, which is in line with the needs identified in the government mission "The basis for a long-term competence supply in the field of radiation safety" (SSM2017-134-23). SSM intends to use the results as much as possible within permit review and supervision and disseminate the information to authorities that regulate similar activities.

Need for further research

Since the dosimetry of radioactive aerosols in man is closely linked to the size of the aerosol particles, it is recommended to further investigate the possibility of direct alpha spectrometry after collection with systems that fractionate the aerosols by size (impactor systems). The interferences in alpha spectra from other types of radiation needs to be further investigated (e.g. coincidences between alpha and other types of ionizing radiation, or the influence of other types of ionizing radiation registered in the alpha detector). Further estimates of the probable size of ^{148}Gd -containing aerosols generated at different conditions at the ESS are also needed to evaluate the potential of direct alpha spectrometry.

Project information

Contactperson SSM: Karin Aquilonius

Reference: SSM2021-787/ 4530523

Alpha spectrometry of radioactive aerosols from the European Spallation Source – an investigation of the possibilities of direct alpha spectrometry

Kristina Eriksson Stenström¹, Guillaume Pédehontaa-Hiaa^{2,1},

Belikse Ramljak¹, Christopher L Rääf²

¹Lund University, Department of Physics, Division of Nuclear Physics

²Lund University, Department of Translational Medicine, Medical Radiation
Physics, Malmö

Summary

The pure alpha emitter ^{148}Gd is considered to be of particular importance from a radiation protection point of view in the event of an accident at the European Spallation Source (ESS), a neutron-generating facility which is under construction on the outskirts of Lund in southern Sweden. In the dimensioning event described in the Swedish Radiation Safety Authority's report SSM2018:02, and which is the basis for placement of the ESS facility in threat category II, the inhalation dose is attributed to more than 50% of the effective dose during the first 7 days after the accident. More than half of the total effective dose during this period originates from ^{148}Gd (half-life=71.1 y; E_{α} =3183 keV). Even during normal operation, small amounts of ^{148}Gd and other radioactive nuclides may be released into the environment via stacks connected to the ESS facility's ventilation system. For correct dose estimates, techniques to measure ^{148}Gd in ambient samples are needed. Since ^{148}Gd is expected to appear in aerosol form and since the inhalation dose is of the greatest importance, collection of airborne aerosols in air is suitable.

One aim of this report is to describe some of the basic requirements for being able to quantify ^{148}Gd in aerosol samples collected from ambient air of the ESS on filters using special air samplers, both during normal operation and at an accident scenario. The focus is on evaluating the possibility of direct alpha spectrometry, where the alpha radiation from the filter sample is measured without pretreatment. By excluding traditional chemical extraction of alpha emitters of interest, environmental monitoring may become significantly more labor- and cost-effective. One goal of the report is to evaluate what type of air sampler, filter material, air flow rates, and collection periods would be suitable for subsequent direct alpha spectrometry.

Radioactive aerosols in the surroundings of the ESS facility will be monitored during operation with the help of several high-flow collection systems, which will collect aerosols on filters (typically weekly samplings), and then, among other things, the activity from gamma-emitting radionuclides will be measured. Part of this report describes whether this type of sampling system is useful for direct alpha spectrometry. As the ESS facility's aerosol samplers are not yet installed, a similar high-flow collection system located at the rural background station Hyltemossa (located 46 km NNE of Lund) has instead been investigated. Naturally occurring alpha-emitting radionuclides (radon daughters) were studied in the filters, partly to provide information on the characteristics of the alpha spectra e.g. as a function of the thickness of the collected aerosol layer and the alpha activity as a function of time after end of sampling, and partly to estimate possible interference from natural alpha emitters on future aerosol samples collected around the ESS.

The analysis of the filters shows that most of the alpha activity from the radon progenies on the filters has vanished after a few days, and that ^{210}Po (half-life =138 d; E_{α} =5304 keV) can be clearly seen in filters analyzed several months after the end of collection. The high-flow collection system used proved unsuitable for direct alpha spectrometry due to slowing down (straggling effects) of the alpha particles in the excessively thick collected layer of aerosols. An estimate of the thickest suitable aerosol layer is presented, as well as suggestions

for suitable airflows and collection times that may enable direct alpha spectrometry of aerosol samples collected on filters for environmental monitoring purposes and as emergency preparedness in case of accidental releases.

The report also uses estimated emission data combined with dispersion calculations in both normal operation and in the dimensioning event of accidental releases to simulate basic alpha spectra (using the program AASI) from aerosol samples collected on membrane filters. If several days pass between the end of aerosol collection and the alpha spectrometry measurement, short-lived ESS-derived radionuclides have time to decay and ^{148}Gd is expected to be the predominant ESS-attributed alpha activity. The energy resolution will not only depend on the thickness of the aerosol layer, but also on the size of the aerosol particles and the extent to which they penetrate the filter. Best energy resolution is obtained for thin layers ($< 200 \mu\text{g cm}^{-2}$), small particles ($\ll 1 \mu\text{m}$ in diameter) and non-existent penetration in the filter. Low collection flows are therefore necessary. Since the dosimetry of radioactive aerosols in man is closely linked to the size of the aerosol particles, it is recommended to further investigate the possibility of direct alpha spectrometry after collection with systems that fractionate the aerosols by size (impactor systems).

In this report, interferences in alpha spectra from other types of radiation have not been taken into account (e.g. coincidences between alpha and other types of ionizing radiation, or the influence of other types of ionizing radiation registered in the alpha detector). This needs to be done in future investigations before it is possible to assess whether direct alpha spectrometry is possible for aerosols collected in an accident scenario at ESS or in environmental monitoring at normal operating conditions. Further estimates of the probable size of ^{148}Gd -containing aerosols generated at different conditions at the ESS are also needed to evaluate the potential of direct alpha spectrometry.

Sammanfattning

Den rena alfastrålararen ^{148}Gd (fysikalisk halveringstid=71 år; $E_\alpha=3183$ keV) anses vara av särskild vikt ur strålskyddssynpunkt vid eventuella olyckstillbud vid Europeiska Spallationskällan (ESS), som är under uppbyggnad i utkanten av Lund i södra Sverige. Vid den dimensionerande händelsen som beskrivs i Strålsäkerhetsmyndighetens rapport SSM2018:02 och som ligger till grund för placering i beredskapskategori II, uppskattas inandningsdosen utgöra mer än 50% av den effektiva dosen under de första 7 dyggen. Mer än hälften av den totala effektiva dosen under denna tid härstammar från ^{148}Gd . Även vid normal drift kan små mängder ^{148}Gd och andra radioaktiva nuklider släppas ut till omgivningen via skorstenar kopplade till ESS-anläggningens ventilationssystem. För korrekta dopsuppskattningar behöver därför ^{148}Gd kunna mätas i omgivningsprover. Eftersom ^{148}Gd förväntas uppträda i aerosolform och eftersom inandningsdosen är av så stor betydelse, bör provtagning i omgivningen lämpligen fokusera på insamling av luftburna aerosoler.

Ett mål med denna rapport är att redogöra för en del av grundförutsättningarna för att kunna kvantifiera ^{148}Gd i aerosolprov som insamlats på filter från luft i omgivningarna till ESS med hjälp av speciella luftprovtagare, såväl under normal drift som vid ett olycksscenario. Fokus ligger på att undersöka möjligheten för direkt alfaspektrometri, där man utan förbehandling mäter alfastrålningen från filterprovet. Genom att utesluta traditionell kemisk extraktion av aktuell alfastrålarare öppnas möjligheter för en mer arbets- och kostnadseffektiv miljöövervakning. Ett mål med rapporten är att utvärdera vilken typ av luftprovtagare, filtermaterial, luftflöden och insamlingsperioder som skulle lämpa sig för efterföljande direkt alfaspektrometri.

Radioaktiva aerosoler i omgivningen till ESS-anläggningen kommer under drift att övervakas med hjälp av flera högflödesinsamlingssystem, som kommer att samla aerosoler på filter (typiska insamlingstider ca 1 vecka åt gången), och där sedan bl. a. aktiviteten från gammastrålande radionuklider kommer att mätas. En del av denna rapport beskriver huruvida denna typ av insamlingssystem är användbart för direkt alfaspektrometri. Eftersom ESS-anläggningens aerosolprovtagare ännu inte är installerade har i stället ett liknande högflödesinsamlingssystem lokaliserat på den rurala bakgrundsstationen Hyltemossa (belägen 46 km NNE om Lund) undersökts. Naturligt förekommande alfastrålande radionuklider (radondöttrar) studerades i filtren, dels för att ge information om alfaspektrens karakteristika som funktion av t. ex. tjockleken på insamlat aerosollager och tid efter avslutad provinsamling, och dels för att uppskatta möjlig interferens från naturliga alfastrålarare på kommande aerosolprov insamlade runt ESS. Analysen visar att merparten av alfaaktiviteten från radondöttrarna på filtren har avklingat efter några dagar, och att ^{210}Po (halveringstid =138 dygn; $E_\alpha=5304$ keV) kan ses tydligt i filter som analyserats flera månader efter avslutad insamling. Det använda högflödesinsamlingssystemet visade sig emellertid olämpligt för direkt alfaspektrometri pga uppbromsning av alfapartiklarna i ett alltför tjockt insamlat lager av aerosoler. En uppskattning av tjockast lämpliga aerosollager presenteras, samt förslag på lämpliga luftflöden och insamlingstider som eventuellt kan möjliggöra direkt alfaspektrometri av aerosolprov insamlade på filter i miljöövervakningssyfte.

Rapporten använder dessutom uppskattade utsläppsdata kombinerat med spridningsberäkningar vid såväl normal drift av ESS som vid den dimensionerade olyckshändelsen för att med programmet AASI simulera grundläggande alfaspektra från aerosolprov insamlade på filter. Om flera dagar förlöper mellan avslutad aerosolinsamling och alfaspektrometrimätningen hinner kortlivade radionuklider från ESS att avklinga och ^{148}Gd förväntas dominera det totala ESS-bidraget av alfaaktiviteten i filtret. Energiupplösningen kommer inte enbart att bero på aerosollagrets tjocklek, men även på aerosolpartiklarnas storlek och till vilken grad de tränger ner i filtret. Bäst energiupplösning erhålls för tunna skikt ($< 200 \mu\text{g cm}^{-2}$), små partiklar ($\ll 1 \mu\text{m}$ i diameter) och obefintlig nedträngning i filtret. Låga insamlingsflöden är därför nödvändiga. Eftersom stråldoser till människor för radioaktiva aerosoler är starkt kopplade till aerosolpartiklarnas storlek rekommenderas att kommande undersökningar utreder möjligheten till direkt alfaspektrometri efter insamling med system som fraktionerar aerosolerna efter storlek (impaktorsystem).

Innan det går att bedöma om direkt alfaspektrometri är möjlig för aerosoler vid luftprovtagning vid ESS behöver ytterligare studier också göras över störningar i alfaspektra från andra typer av strålning (t ex koincidenser mellan alfa och andra joniserande strålningstyper, eller påverkan från andra typer av joniserande strålning som registreras i alfadetektorn). Dessutom behövs ytterligare uppskattningar av sannolika partikelstorlekar på ^{148}Gd -innehållande aerosoler som genereras vid olika förhållanden vid ESS för att utvärdera potentialen för direkt alfaspektrometri vid miljöövervakning och beredskapsmätningar.

Abbreviations and notations

| | |
|---------------|---|
| AMAD | Activity median aerodynamic diameter |
| AMTD | Activity median thermodynamic diameter |
| BR | Branching ratio |
| EC | Electron capture |
| ESS | European Spallation Source |
| HiVol sampler | High-volume sampler |
| HRTM | Human respiratory tract model |
| HATM | Human alimentary tract model |
| MDAC | Minimum detectable activity concentration |
| PM | Particulate matter |
| PM10 | Airborne particles with diameter < 10 μm |
| SSM | Swedish Radiation Safety Authority |
| ST | Source term |
| TSP | Total suspended particulate matter |
| UFP | Ultrafine particles |

Contents

| | |
|--|-----------|
| 1. Introduction | 8 |
| 2. Aerosols – a brief introduction..... | 10 |
| 3. Alpha spectrometry of aerosols..... | 13 |
| 3.1. Aerosol sampling | 13 |
| 3.2. Direct alpha spectrometry..... | 13 |
| 4. Gaussian plume modelling of momentary ground level concentrations around the ESS | 16 |
| 4.1. Introduction | 16 |
| 4.2. ESS-specific parameters | 19 |
| 5. Aerosol alpha spectra during normal operation | 22 |
| 5.1. Aerosol releases from the ESS during normal operation | 22 |
| 5.1.1. Predicted total release rates..... | 22 |
| 5.1.2. Estimates of ^{148}Gd and W in air..... | 23 |
| 5.2. Alpha spectra from the rural reference site Hyltemossa . | 25 |
| 5.3. Simulation of aerosol spectra from normal operation | 41 |
| 5.3.1. Case 1: ^{210}Po in homogenous source of aerosols | 43 |
| 5.3.2. Case 2: Radioactive particles in a homogenous source matrix | 44 |
| 5.3.3. Case 3: Effect of particle size | 46 |
| 5.3.4. Comparison with measured spectrum..... | 46 |
| 5.3.5. Notes on suitable aerosol sampling flow rates | 46 |
| 5.3.6. Hypothetical alpha spectrum from normal operation of the ESS | 47 |
| 5.4. Conclusions | 48 |
| 6. Aerosol alpha spectra during an accident scenario | 49 |
| 6.1. The AA3 accident scenario..... | 49 |
| 6.2. Aerosol alpha spectra at the AA3 accident scenario | 53 |
| 6.3. Conclusions | 57 |
| 7. Summary and conclusions | 58 |
| 8. Acknowledgement | 60 |
| 9. References..... | 61 |
| Appendix 1..... | 65 |
| Appendix 2..... | 67 |

1. Introduction

In case of an accidental release of target material from the tungsten wheel of the European Spallation Source (ESS), different exposure pathways of radionuclides to man must be considered for dose assessments of workers and members of the public. An important exposure pathway is inhalation of gases and aerosols (liquid or solid particles suspended in air). The pure alpha emitter ^{148}Gd in aerosol form is believed to be of particular relevance, as reported by the Swedish Radiation Safety Authority (SSM) in a report which classifies ESS facility as a threat category II facility [1]. Methods to analyse the concentration of ^{148}Gd in ambient air are therefore needed. Releases of radioactive aerosols may also occur during normal operation of the facility, and therefore assessment of inhalation of alpha emitters in aerosol form is needed. Estimation of radioactive releases can be done through environmental monitoring to ensure that the dose limits to public are not exceeded.

The main aim of this document is to evaluate the feasibility of direct alpha spectrometry of aerosol-laden filters obtained from aerosol samplers in the vicinity of the ESS in case of the emergency scenario described in the SSM report SSM2018:02 [1]. The advantage of direct alpha spectrometry compared to traditional alpha spectrometry is that the laborious and time-consuming chemical extraction of the relevant elements is omitted. The ESS will continuously operate high-volume (HiVol) aerosol samplers located outdoors at the site. These samplers will collect aerosols on filters using a high flow rate (60 to $90\text{ m}^3\text{ h}^{-1}$) for up to one week prior to filter change. Gamma-spectrometric analysis will benefit from the high flowrate, and hence the relatively higher amounts of sample material than if low flow rates were used. Direct alpha spectrometry may however be disadvantaged by the straggling effects (loss of kinetic energy, or complete absorption) of alpha particles in the layer of sampled aerosols, leading to total counting loss of some of the alpha particles or to extensive broadening of the energy peaks. Coincidences between the alphas and other ionising radiation types (beta particles, electrons, and low-energy photons) may also distort the spectrum. This report is a first step towards designing a suitable aerosol collection system for direct alpha spectrometry that can be used for environmental monitoring during normal operation at the ESS as well as during a potential accident.

The report aims to provide the reader with a brief general introduction to naturally occurring and man-made radioactive aerosols, in particular alpha-emitting aerosols, and their sampling and analytical techniques. Based on information on the magnitude of potential releases of alpha-emitting aerosols during normal operation and at a specific accident scenario, the maximum ground-level concentration in air is estimated using a simplified Gaussian plume modelling approach. The report presents a first set of simplified simulations of alpha spectra from aerosols collected with aerosol samplers at the location of maximum activity concentration. Optimal flowrates and collection times are discussed. The report also presents direct alpha spectrometry measurements of aerosol-laden filters collected with a HiVol sampler at a rural background station (Hyltemossa, near Perstorp in southern Sweden). These measurements

serve to demonstrate background alpha spectra for HiVol filters with various aerosol loading and at different times after end of aerosol collection.

The simplified approaches in this report (i.e., not including e.g. coincidences between the alphas and other ionizing radiation types, or the influence from other types of ionizing radiation registered in the alpha detector) prevent the full decision on whether direct alpha spectrometry of aerosol samples collected in ambient air around the ESS is feasible or not. However, the report provides relevant information that can be used in more extended and detailed simulations of anticipated energy spectra obtained from direct alpha spectrometry at normal operation as well as an accident scenario at the ESS.

2. Aerosols – a brief introduction

This chapter provides a very brief introduction to aerosols in general and radioactive aerosols in particular. The chapter ends with a short notice on the dosimetry of radioactive aerosols.

Aerosols in the environment have natural as well as anthropogenic origin. Natural aerosols include e.g. pollen, bacteria, fungal spores, sea-spray, wildfires and oxidized products of gas-phase volatile organic compounds emitted from plants. Anthropogenic aerosols may originate from e.g. various combustion processes and traffic wear on roads. The chemical composition of aerosols has significant temporal as well as spatial variations, and includes organic carbon, elemental carbon, sulphate, nitrate, ammonium, and various trace elements [2, 3]. Aerosol particles stay in the atmosphere for various residence times, spanning from days (near the surface of earth) to years (in the stratosphere).

The size of aerosols varies over a large range, from a fraction of a μm to hundreds of μm . The size distributions of atmospheric aerosols are often bimodal, and aerosols are referred to as coarse particles (diameter $> 1 \mu\text{m}$) and fine particles (diameter $< 1 \mu\text{m}$). Coarse particles mainly originate from mechanical processes, whereas the fine particles stem from condensation of gases. The coarse particle mass fraction is usually larger than the fine fraction. The size of some types of aerosol particles may grow over time due to condensation or coagulation. The aerosol particle may thus have been transformed from its initial appearance at formation and emission to the environment, until sampled by an aerosol sampling device (or until inhaled by humans). It may also have disappeared from the atmosphere before reaching the sampler, e.g. through contact with a surface or washout by rain. Radioactive nuclei in aerosols may also have decayed before being sampled and measured.

Another classification of aerosols is considering the fate of the aerosols when inhaled by humans. Aerosols of diameter $> 10 \mu\text{m}$ do not enter the lungs as the nose and upper airways act as filters for these large particles (these particles will eventually be swallowed). Particles with a diameter of $< 10 \mu\text{m}$ (PM₁₀) can however enter the lower airways, and the smaller the particles, the deeper penetration and deposition in the respiratory tract. Particulate matter with diameter of about $10 \mu\text{m}$ accumulates mainly in the conducting airways, particles with diameter $< 2.5 \mu\text{m}$ can also enter the terminal bronchioles, whereas ultrafine particles (UFP, diameter $< 0.1 \mu\text{m}$) reach the alveoli from where the UFPs may diffuse into the bloodstream and be further transported to other organs in the body [4]. Particles deposited not as deep in the lungs as the UFPs are transported to the throat and swallowed.

The size of aerosols is sometimes referred to in terms of aerodynamic diameter and AMAD (Activity Median Aerodynamic Diameter). The aerodynamic diameter of a particle is defined as that of a sphere of density 1 g cm^{-3} (i.e., the density of water), which settles in still air at the same velocity as the particle in question. AMAD is used to attribute certain aerodynamic behavior to the aerosol and refers to its physical size. AMAD is used with the aim to estimate the log

normal distribution of an aerosol activity size with a single value (median value). It is determined as the value of the aerodynamic diameter for which 50% of the activity of the aerosol is associated with particles smaller than the AMAD, and 50% of the activity is associated with particles larger than the AMAD [5]. AMAD is used for particle sizes > about 0.5 μm (sedimentation and inertial impaction dominate the deposition of the particles). For smaller particles, the term Activity Median Thermodynamic Diameter (AMTD) is used instead (diffusion dominates the deposition mechanism; the thermodynamic diameter is the diameter required for a spherical particle of density 1 g cm^{-3} to have the same diffusion coefficient as the particle on interest [5]).

As stated above, the spatial and temporal variation in the concentration of aerosols vary significantly. The annual average concentration of PM10 in rural areas in southern Sweden is typically about 10 $\mu\text{g m}^{-3}$ [6]. The total suspended particulate matter (TSP) concentration may be approximated as being twice as high as the PM10 concentration [7], but variations in this ratio can be substantial [8]. The legislative maximum PM10 concentration that should not be exceeded is 40 $\mu\text{g m}^{-3}$ on an annual basis and 50 $\mu\text{g m}^{-3}$ on a daily basis¹.

Natural as well as anthropogenic aerosols also contain radioactive nuclides. Naturally occurring radionuclides, partly present in aerosol form are e.g. cosmogenic ^{14}C (pure β^- ; $T_{1/2} = 5730$ y, present in all organic compounds of non-fossil origin) [9-12], ^7Be (EC; $T_{1/2} = 53.3$ d), ^{210}Pb (β^- ; $T_{1/2} = 22.2$ y), ^{212}Pb (β^- ; $T_{1/2} = 10.6$ h), ^{22}Na (EC, β^+ ; $T_{1/2} = 2.6$ y), ^{35}S (β^- ; $T_{1/2} = 87.4$ d), ^{32}P (β^- ; $T_{1/2} = 14.3$ d) and ^{33}P (β^- ; $T_{1/2} = 25.4$ d).

Radioactive aerosols in ambient uncontaminated air include decay products from ^{222}Rn (radon) in the uranium series, ^{223}Rn (actinon) in the actinium series and ^{220}Rn (thoron) from the thorium series. Many of the Rn daughters are alpha emitters (see Figure 1 illustrating the main decays of the uranium series). More detailed information about half-lives and branching ratios for the uranium series, the actinium series and the thorium series can be found in Appendix 1. Alpha energies for the main decays from radon progenies are listed in Appendix 2.

The radon concentration in outdoor air is typically between 1 and 100 Bq m^{-3} (average ~ 10 Bq m^{-3}) while soil gas usually has 3-4 orders of magnitude higher radon activity concentrations [13]. Indoor radon concentrations vary from a few Bq m^{-3} to several tens of kBq m^{-3} [13]. Diurnal and seasonal variations in radon concentration may be significant outdoors as well as indoors.

In outdoor as well as in indoor air, the radon daughters may be in attached or in unattached form. The attached fraction has typical sizes of 0.01-1 μm and include radon progenies attached to already existing aerosol particles. The unattached fraction has typical sizes of 0.5-5 nm and consist of radon progenies that have reacted with air vapour and trace gases.

The fate and dosimetry of inhaled radioactive aerosols (for occupational exposure) is described by the ICRP (International Commission of Radiological Protection) by the human respiratory tract model (HRTM) (see [14-16] and references therein). The dosimetry of particles transported from the airways to the alimentary tract (i.e. particles swallowed) is described by the human

¹ Sveriges Riksdag, Luftkvalitetsförordning (2010:477) 18 §.

alimentary tract model (HATM) [14-16]. The dosimetry depends not only on the elemental and chemical form of the particles inhaled, but also on particle size distribution and biokinetics of the nuclide [14-16]. ICRP classifies different types of particulate matters into four categories depending on the rate at which they are absorbed into blood from the respiratory tract; type V representing a very fast rate, type F a fast rate, type M for moderate rate, and type S, which are more insoluble materials that have a slow rate of absorption. The different classes will thus affect the inhalation dose coefficients to the exposed subject. Further information about the classification and committed effective doses from inhaled ^{148}Gd can be found in Rääf et al [17].

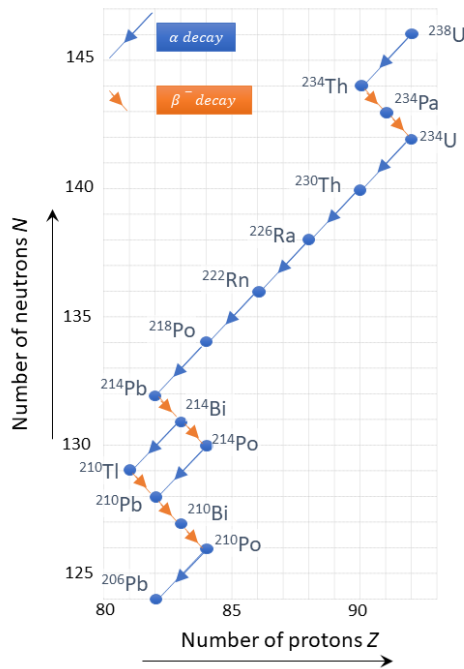


Figure 1 The main decays of the uranium series. The radionuclides in the decay chain from ^{238}U to ^{226}Ra are solids, ^{222}Rn is a gas, and the radon daughters (radionuclides in the decay chain from ^{218}Po to ^{206}Pb) will appear as aerosols.

In the dispersion and dose calculations for the dimensioning event, as presented by SSM [1], an AMAD of $1\ \mu\text{m}$ was used, whereas in the study by Rääf et al [17] instead used a particle size of $\text{AMAD} = 2.2\ \mu\text{m}$, as it represented better the only human experiments conducted on Gd-inhalation [18]. The latter yielded a committed effective dose of $1.26 \cdot 10^{-5}\ \text{Sv}$ per unit inhaled Bq ^{148}Gd for an adult, which is about a factor of two less than that for a type F (fast absorption rate) particle in the size range $1\ \text{to}\ 5\ \mu\text{m}$, but somewhat higher than the corresponding values for type M particles in the same size range.

3. Alpha spectrometry of aerosols

This chapter briefly introduces the concepts of aerosol sampling and direct alpha spectrometry.

3.1. Aerosol sampling

A variety of aerosol samplers exist commercially, using a pump to draw air through an inlet port towards an aerosol trap consisting of a filter or a surface. The sampler is usually equipped with a flow meter to assess the volume of air that has passed the aerosol trap. The size and flowrates of various radioactive aerosol samplers range from miniature low-volume samplers for individual monitoring of workers (flowrates of single L min^{-1}), to large HiVol samplers (flow rates up to several tens of $\text{m}^3 \text{min}^{-1}$). Alpha continuous air monitoring (alpha-CAM) devices have an alpha-radiation detector system positioned coaxially over the filter to obtain real-time data [19]. Other systems sample aerosols over a defined period (days-weeks) prior to off-line analysis. Samplers can be equipped with inlets removing the larger particles (e.g. PM10 inlets, excluding particles with a diameter of $> 10 \mu\text{m}$). So called impactors can collect the aerosols in size fractions [20, 21].

HiVol samplers are advantageous in environmental monitoring of gamma emitters, and the larger the mass sampled on the filter, the lower the minimum detectable activity concentration (MDAC). HiVol samplers usually operate for several days prior to filter change, and thus results in relatively thick samples (depending on the filter area and the aerosol concentration in air).

Assessment of individual exposures to radioactive aerosols can be performed using personal air sampling devices or static air sampling devices [14]. The personal air sampler is a small device carried by the worker, collecting aerosols on filters using flowrates of about one-fifth of normal breathing rates (the latter about $1.2 \text{ m}^3 \text{h}^{-1}$) [14]. Personal air samplers may also be equipped with cascade impactors to obtain different size fractions of aerosols. For example, in recent studies of uranium aerosol exposure at Westinghouse nuclear fuel fabrication plant in Sweden, a flowrate of $0.12 \text{ m}^3 \text{h}^{-1}$ was used to obtain size fractions of $> 21.3 \mu\text{m}$, $21.3\text{-}14.8 \mu\text{m}$, $14.8\text{-}9.8 \mu\text{m}$, $9.8\text{-}6.0 \mu\text{m}$, $6.0\text{-}3.5 \mu\text{m}$, $3.5\text{-}1.6 \mu\text{m}$, $1.6\text{-}0.9 \mu\text{m}$ and $0.9\text{-}0.5 \mu\text{m}$ [22-24]. An end-stage filter collected remaining particles after all impaction stages [22-24].

3.2. Direct alpha spectrometry

Alpha spectrometry of aerosol samples on filters may be performed using Si semiconductor detectors (also called PIPS, Passivated Implanted Planar Silicon detectors) after radiochemical separation and production of thin targets, or using gas ionization detectors or liquid scintillation counting (LSC) (e.g. [25, 26]). Direct high-resolution alpha spectrometry of aerosol filters without radiochemical sample treatment has also been demonstrated,

e.g. by Pöllänen et al [27, 28]. Direct alpha spectrometry is attractive for emergency preparedness as well as for other monitoring situations, due to the omission of the time- and labour-consuming chemical extraction procedures [29].

Direct alpha spectrometry is not trivial, e.g. due to the high stopping power of alphas, which may lead to self-absorption in the sample and broadened peaks in the energy spectrum. The thinner the samples, the better, is a general rule in alpha spectrometry, provided that the counting statistics will not be a limiting factor. The size and density of the radioactive particle itself also affect the self-absorption of emitted alpha particles. Straggling losses in the filter material due to penetration of collected particles into the filter may also be problematic. Choice of filter type is thus important to minimize losses of alpha particles in the filter [19]. Membrane filters are known to be suitable for alpha spectrometric measurements [28].

The presence of many different radionuclides and radiation types may also be cumbersome for direct alpha spectrometry. Coincidences between alpha particles and beta particles, electrons and low-energy photons may need to be considered [30]. Pöllänen and Siiskonen considered two types of coincidences in a paper using direct alpha spectrometry to investigate alpha spectra from a membrane filter containing radon daughters [30]. The first type of coincidence is due to conversion electrons, Auger electrons or low-energy photons promptly emitted from excited daughter nuclei, where the pulse shaping time of the electronics of the detector system exceeds the lifetime of the excited states of the daughter nuclide [30]. The second type of coincidence may arise for short-lived alpha-emitters with half-lives of the same range as the time resolution of the electronics: coincidence may then occur between the alphas and beta particles or other radiation types emitted from various radionuclides in the sample [30].

In [31], Pöllänen and Siiskonen investigate the possibility to identify alpha emitters from air samples with direct alpha spectrometry in the case of samples containing many different radionuclides. They report that direct alpha spectrometry of membrane filter samples from nuclear fuel particles in outdoor air can be successful, given that the radioactive particles are on the sample surface, that their size is small (diameter $\ll 1 \mu\text{m}$) and that a spectrum analysis code is developed to unfold the resulting complex alpha spectra. The low-energy tail of the alpha particle peaks is highly depending on the degree of penetration into the air filter. Additionally, the presence of some natural radionuclides (radon progenies) needs to be included in the spectrum analysis [31]. Pöllänen and Siiskonen also claim that for particle sizes considerably smaller than $1 \mu\text{m}$, alpha peaks separated by $>50 \text{ keV}$ can be resolved for membrane filters. Other examples can be found in the literature where direct alpha spectrometry has been used for environmental samples, e.g. from the Chernobyl accident (see [31] and references therein).

According to other studies by Pöllänen et al [27, 32, 33], the presence of alpha emitting actinides in air filters may be identified to the level of 0.1 Bq m^{-3} using direct alpha spectrometry. The same group has reported high-resolution alpha spectrometry measurements and modelling at ambient air pressure using collimators [34]. They claim that contamination of 1 Bq cm^{-2} on any smooth and flat surface can be detected in approximately 10 s data acquisition time, but

longer times are needed for radionuclide identification. Moreover, the possibility to detect beta-emitting radionuclides using the same measurement technique was also reported. Counts originating from alpha and beta particles are mainly at different energies, which make their separation possible. An efficiency of 0.14 was determined for an extended-area (430 cm²) homogeneous source emitting alpha radiation at the energy of 5–6 MeV, whereas for the beta emitters the efficiencies were 0.07–0.19 depending on the beta-particle emission energies. The use of a collimator reduced the detection efficiencies by a factor of up to ten [35]. The effect of collimators, as well as peculiarities of alpha spectra in aerosol filters have also investigated by other authors [36, 37].

4. Gaussian plume modelling of momentary ground level concentrations around the ESS

This chapter includes conservative estimates of the maximum ground-level activity concentration that can be expected from radioactive releases from the main stack and the waste stack of the ESS.

4.1. Introduction

To estimate activity levels of aerosols collected on filters in the vicinity of the ESS facility, estimates of the ground-level activity concentration are needed. The most general form of Gaussian plume model [38] was used to perform a very rough estimate of the ground-level concentration resulting from the releases (both nonradioactive and radioactive) from ESS stacks. The model does not take gravitational settling of particles into account - neither the effect on the dispersion due to large buildings and surface roughness - and states that the momentary ground level concentration C of an air pollutant in the downwind direction at a distance x from the source is given by:

$$C = \frac{Q}{\pi \sigma_y \sigma_z u} \cdot e^{-\frac{H_e^2}{2\sigma_z^2}} \quad (1)$$

where

- C ground-level concentration of the pollutant (e.g. in Bq m⁻³ or g m⁻³)
- σ_y horizontal dispersion coefficient, characterized as the standard deviation of the concentration distribution in the crosswind direction at downwind distance x from the source (m)
- σ_z vertical dispersion coefficient, characterized as the standard deviation of the concentration distribution in the vertical direction at downwind distance x from the source in (m)
- Q release rate (e.g. in Bq s⁻¹ or g s⁻¹)
- H_e effective stack height (m)
- u mean horizontal air velocity (m s⁻¹) at the release height

The effective stack height may be approximated by [39]:

$$H_e = h + d \cdot \left(\frac{v}{u}\right)^{1.4} \cdot \left(1 + \frac{\Delta T}{T}\right) \quad (2)$$

where

- H_e effective stack height (m)

| | |
|------------|---|
| h | physical stack height (m) |
| d | chimney outlet diameter (m) |
| v | exit velocity of effluent (m s^{-1}) |
| u | mean horizontal air velocity (m s^{-1}) |
| T | temperature of effluent gas (K) |
| ΔT | difference between effluent and ambient temperature (K) |

The dispersion coefficients (σ_y and σ_z) depend on atmospheric conditions which usually are categorized by atmospheric stability classes (also known as Pasquill stability classes), see Table 1 and Table 2.

Table 1 Pasquill stability classes

| Stability class | Conditions |
|-----------------|--------------------------------|
| A | Extremely unstable conditions |
| B | Moderately unstable conditions |
| C | Slightly unstable conditions |
| D | Neutral conditions |
| E | Slightly stable conditions |
| F | Moderately stable conditions |
| G | Extremely Stable |

Table 2 Meteorological conditions defining Pasquill stability classes². Strong insolation refers to sunny midday in summer; slight insolation to sunny midday in winter. The neutral category D is used for overcast conditions during day or night for all wind speeds. Category D is also for one hour at sunrise and one hour at sunset. *Some references, such as Slade (1968) and Cooper et al. (2003) cite different conditions.

| Surface wind speed (m/s) | Daytime insolation | | | Night-time conditions | |
|--------------------------|--------------------|----------|--------|----------------------------------|-------------------|
| | Strong | Moderate | Slight | Thin overcast or > 4/8 low cloud | <= 4/8 cloudiness |
| < 2 | A | A - B | B | E (*G) | F (*G) |
| 2 - 3 | A - B | B | C | E | F |
| 3 - 5 | B | B - C | C | D | E |
| 5 - 6 | C | C - D | D | D | D |
| > 6 | C | D | D | D | D |

The dispersion coefficients σ_y (m) and σ_z (m) can be estimated from ([40] and references therein):

$$\sigma_y = \frac{k_1 x}{\left(1 + \frac{x}{k_2}\right)^{k_3}} \quad (3)$$

$$\sigma_z = \frac{k_4 x}{\left(1 + \frac{x}{k_2}\right)^{k_5}} \quad (4)$$

with constants according to Table 3. σ_y and σ_z as a function of distance x for various Pasquill stability classes is graphically presented in Figure 2.

² [READY Tools - Pasquill Stability Classes \(noaa.gov\)](https://www.noaa.gov/pasquill-stability-classes)

Table 3 Constants for calculation of dispersion coefficients σ_y and σ_z (and other parameters). From ([40] and references therein).

| Stability class | k_1 | k_2 | k_3 | k_4 | k_5 |
|-----------------|--------|-------|-------|--------|--------|
| A | 0.250 | 927 | 0.189 | 0.1020 | -1.918 |
| B | 0.202 | 370 | 0.162 | 0.0962 | -0.101 |
| C | 0.134 | 283 | 0.134 | 0.0722 | 0.102 |
| D | 0.0787 | 707 | 0.135 | 0.0475 | 0.465 |
| E | 0.0566 | 1070 | 0.137 | 0.0335 | 0.624 |
| F | 0.0370 | 1170 | 0.134 | 0.0220 | 0.700 |

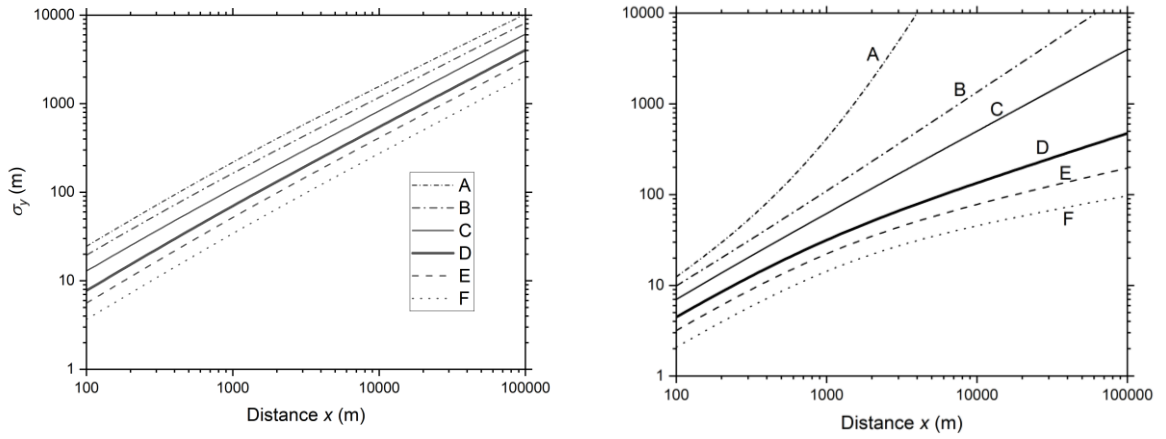


Figure 2 Dispersion coefficients σ_y and σ_z as a function of distance to source x for various Pasquill stability classes, according to Equations (3) and (4).

The long-term average activity concentration C_{av} at a distance x in a specific sector n_i from a point source releasing airborne radionuclides can be approximated by the following version of the Gaussian plume model [38]:

$$C_{av} = \sqrt{\frac{2}{\pi}} \frac{\left(\frac{f}{100}\right) Q_{av}}{\left(\frac{2\pi x}{n}\right) \sigma_z u} \cdot e^{-\frac{H_e^2}{2\sigma_z^2}} \quad (5)$$

where

| | |
|----------|--|
| C_{av} | average long-term concentration (Bq m^{-3}) |
| f | frequency of wind directions into the wind sector |
| n | number of wind sectors |
| Q_{av} | average long-term release rate (Bq s^{-1}) |

and x , σ_z , u and H_e are as above.

In the current document, however, the momentary ground level concentration C is used.

4.2. ESS-specific parameters

The parameters for the airborne discharges from the main stack and from the waste facility stack are presented in Table 4 [41].

Table 4 Parameters for airborne discharges from the main stack and from the waste facility building ([41] and Per Roos personal communication (2020-03-12)).

| Parameter | Abbreviation | Main stack | Waste facility stack | Reference |
|---|-------------------------|---------------------------------------|----------------------|--------------------------------|
| Release type | | Continuous and short-time (hot cells) | Short-time | [41] |
| Stack height above ground (m) | h | 45 | 25 | [41] |
| Stack inner diameter (m) | d | 1.7 | 0.787 | [41] |
| Discharge speed (m s^{-1}) | v | 10 (max 16 m s^{-1}) | 8-14 (average 11) | [41] |
| Temperature of effluents (K) | T | 296 | 297 | [41] |
| Difference between effluent and ambient temperature (K) | $\Delta T = T - T_{av}$ | $296 - 283 = 13$ | $297 - 283 = 14$ | Davis weather station [42, 43] |

Wind roses of relevance for the region and the ESS site are presented in Figure 3 (data from 2019) ([41, 43, 44]). For the ESS site in 2019 the most dominant wind direction was WSW (12.3% of the time, average wind speed 4.2 m s^{-1}). Other dominant wind directions were ESE (12.2%, 3.8 m s^{-1}), W (11.6%, 3.8 m s^{-1}) and SW (11.3%, 5.2 m s^{-1}). Average wind speed for all wind directions over the whole year was 3.7 m s^{-1} and the average outdoor temperature in 2019 was $9.8 \text{ }^\circ\text{C}$ ($T_{av} = 10 \text{ }^\circ\text{C} = 283 \text{ K}$ in Table 4).

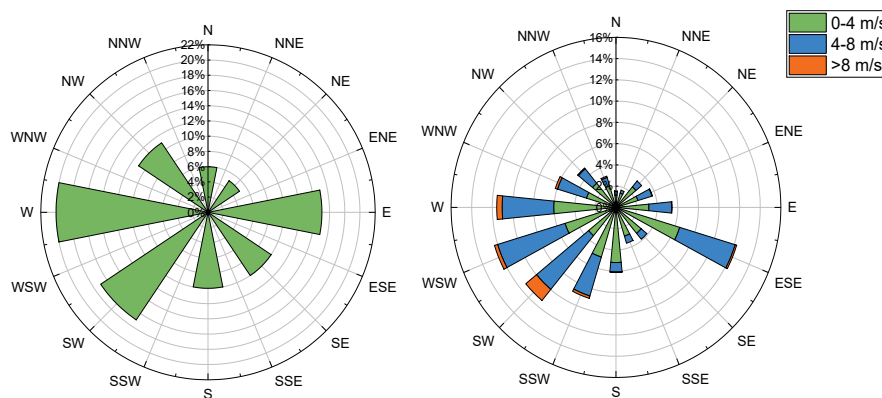


Figure 3 **Left:** Windrose for Malmö-Sturup airport for years 2006-2012 [41]. **Right:** Windrose representative for the location of the ESS facility for year 2019, obtained from hourly measurements at the ESS [42].

The software Origin Pro was used to calculate the momentary downwind normalized concentration C (see above) per unit of release rate, resulting from dispersion of the effluents from the main stack (see Figure 4). The unit on the y-

axis in Figure 4 may also be read as g m^{-3} per g s^{-1} for releases of stable compounds such as WO_3 (e.g. in case of the accident scenario AA3). The wind speed 4.2 m s^{-1} was selected since this was the average wind speed in the main wind direction (WSW) obtained for 2019. Stack air flow rates were assumed to be the same as stack air flow rates during normal operation (see Table 4). All stability classes were included, however, category D (neutral) or C (slightly unstable) seem most relevant for the meteorological conditions at the ESS for daytime when photosynthesis is active in plants (see Table 2).

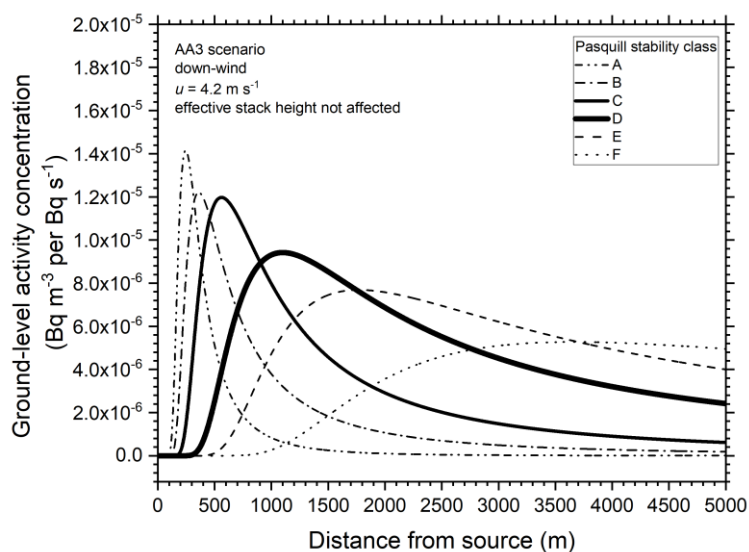


Figure 4 Normalized ground-level activity concentration per unit of release rate from the main stack in the down-wind direction calculated for an air speed of 4.2 m s^{-1} .

The maximum normalized ground-level activity concentration according to the scenario in Figure 4 (relevant to the main wind direction WSW) is $1.2 \cdot 10^{-5} \text{ Bq m}^{-3}$ per Bq s^{-1} and occurs at a downwind distance of 560 m for Pasquill stability class C. The corresponding distance for stability class D is 1100 m and $9.4 \cdot 10^{-6} \text{ Bq m}^{-3}$ per Bq s^{-1} . In the nearest village Odarslöv, located about 1.6 km from the main stack in the main wind direction, the normalized ground-level activity concentrations are $4.1 \cdot 10^{-6} \text{ Bq m}^{-3}$ per Bq s^{-1} for stability class C and $8.2 \cdot 10^{-6} \text{ Bq m}^{-3}$ per Bq s^{-1} for stability class D. These values are somewhat higher compared to calculations presented in the ESS document ESS-0092831 [45]. One reason is that the values presented in the current report are based on the momentary Gaussian plume model in the downwind direction, while the ones in the document ESS-0092831 [45] represent long-term averages, also taking varying wind speeds and wind directions into account.

For the waste stack, the momentary downwind normalized concentration C (see above) per unit of release rate at different Pasquill stability classes, is shown in Figure 5. As in Figure 4, the average wind direction of 4.2 m s^{-1} has been used. The distance from release point to the maximum normalized ground-level activity concentration is smaller for the waste stack than for the main stack, due to the lower height of the waste stack. As a further consequence, the magnitude

of the maximum normalized ground-level activity concentration is higher for the waste stack than for the main stack ($\sim 3.9 \cdot 10^{-5}$ Bq m⁻³ per Bq s⁻¹ and occurs at a downwind distance of 300 m for Pasquill stability class C, and $\sim 3.5 \cdot 10^{-5}$ Bq m⁻³ per Bq s⁻¹ at 530 m for Pasquill stability class D).

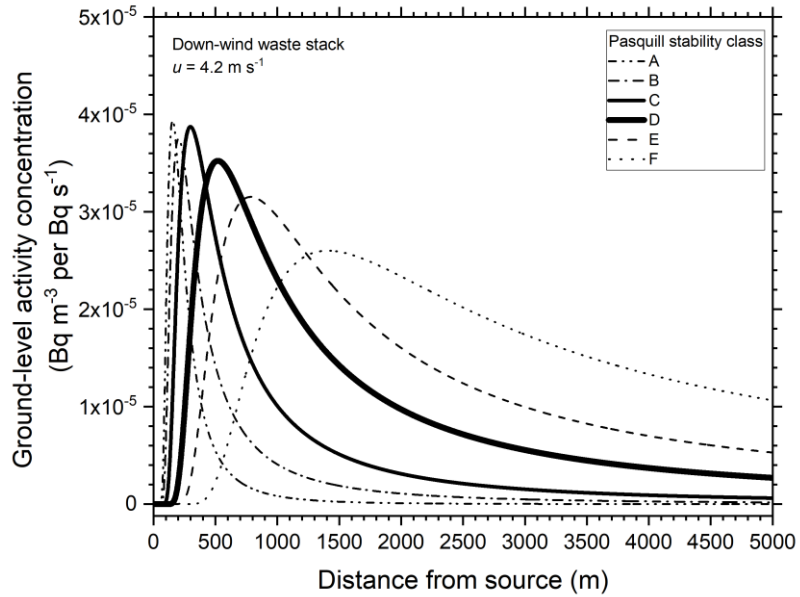


Figure 5 Normalized ground-level activity concentration per unit of release rate from the waste stack in the down-wind direction calculated for an air speed of 4.2 m s⁻¹.

5. Aerosol alpha spectra during normal operation

The expected releases of alpha emitting aerosols from the ESS during normal operation are presented in this chapter. Based on maximum allowed doses for members of the public, a maximum allowed concentration of ^{148}Gd is estimated in the main downwind direction of the ESS. Before simplified simulations of the potential energy spectra that may be obtained from direct alpha spectrometry measurements of filters with aerosols collected at a location with these maximum activity concentrations, alpha spectra from aerosols collected on filters at the rural background station Hyltemossa in southern Sweden are presented and discussed.

5.1. Aerosol releases from the ESS during normal operation

5.1.1. Predicted total release rates

Radioactive aerosols are expected to be formed at several locations at the ESS facility during normal operation. The air of accelerator tunnel is believed to contain e.g. ^7Be , ^{10}Be , ^{24}Na , ^{32}P , ^{33}P , ^{35}S) (see e.g. [46]). None of these are alpha emitters. HEPA filters in the ventilation systems are expected to remove 99.97% of the aerosols [47, 48]. Typical estimated release rates from the linac tunnel to the environment during 6000 hours of continuous operation are in the order of 10^4 to 10^5 Bq y^{-1} for the radionuclides mentioned above [49].

Aerosols are also expected be formed and released from the W target as a result of the spallation reactions, from sputtering and by ablation caused by the He cooling gas [47, 48, 50]. These aerosols may contain alkali metals, alkaline earth metals, boron group elements, transition metals, metalloids and lanthanides. The pure alpha emitter ^{148}Gd belongs to the latter group. Aerosols released from the W target will be transported by the He gas in the cooling loop, which is equipped with filters to trap particulates [48]. Small leakages are expected from the He cooling loop (of about 1 g h^{-1} of the total 23 kg of He) [50]. Aerosols may also be formed in and released during cutting processes (from tungsten and stainless-steel components) in the hot cells [50].

The ESS consortium has estimated the source term (ST) of radionuclides released to the environment from the target station for two cases, one pessimistic case and one optimal case [50]. The He loop (continuous release) contributes with $6.32 \cdot 10^{11}$ Bq y^{-1} to the ST in both cases. Tritium (^3H) shows the highest contribution to the releases ($6.24 \cdot 10^{11}$ Bq y^{-1}). Metalloids constitute $5.32 \cdot 10^7$ Bq y^{-1} and $1.6 \cdot 10^4$ Bq y^{-1} , in the pessimistic and optimal case, respectively [50]. Short-term release of W and stainless steel dust from dismantling in active cells is estimated to be $6.25 \cdot 10^{11}$ Bq y^{-1} [50]. The ST from the waste building is not known, and the physical and chemical forms of several classes of aerosols are difficult to predict [47].

5.1.2. Estimates of ^{148}Gd and W in air

Due to the radiological importance of ^{148}Gd , it is important to be able to assess it in collected aerosol samples. A simple estimate can be made on how much ^{148}Gd may be released on average on an annual basis, assuming that the annual committed dose contribution from inhalation of ^{148}Gd must not exceed $\dot{E} = 0.1$ mSv year⁻¹ (maximum allowed annual dose for members of public, accumulated due to normal releases from a single nuclear or radiation-related facility). As this dose rate is the maximum allowed annual dose for any member of the general public due to normal releases from a single nuclear or radiation-related facility, this would mean that the total allowed annual dose would stem from ^{148}Gd , which is not realistic. However, the calculations below can easily be scaled down to any other lower annual dose.

The calculations below use the simplified assumption that the release rates from the main stack and from the waste stack are continuous and constant over the year, and that the weather conditions and wind directions are constant. The dose assessment is done for an individual spending all the time at a location of the maximum downwind concentration.

The following parameters are used in the simplified estimate:

- Effective dose coefficient for inhalation of ^{148}Gd (1 μm), e , adult members of the public (Table G.1 in [51]):

$$e(\text{Type } F) = 2.6 \cdot 10^{-5} \text{ Sv Bq}^{-1}$$

$$e(\text{Type } M) = 1.1 \cdot 10^{-5} \text{ Sv Bq}^{-1}$$

$$\text{Average: } e = 1.85 \cdot 10^{-5} \text{ Sv Bq}^{-1}$$

- Breathing rate BR (adults, sitting awake [52]):

$$BR(\text{female}) = 0.39 \text{ m}^3 \text{ h}^{-1} \text{ corresponding to } 3500 \text{ m}^3 \text{ year}^{-1}$$

$$BR(\text{male}) = 0.54 \text{ m}^3 \text{ h}^{-1} \text{ corresponding to } 4797 \text{ m}^3 \text{ year}^{-1}$$

$$\text{Average: } BR = 0.465 \text{ m}^3 \text{ h}^{-1} \text{ corresponding to } 4132 \text{ m}^3 \text{ year}^{-1}$$

The inhaled annual maximum activity \dot{A} is then:

- $\dot{A} = \frac{\dot{E}}{e} = 0.1 \text{ mSv year}^{-1} / 1.85 \cdot 10^{-5} \text{ Sv Bq}^{-1} = 5.4 \text{ Bq year}^{-1}$

The maximum allowed activity concentration in air C is then given by:

$$C(^{148}\text{Gd}) = \frac{\dot{A}}{BR} = 5.4 \text{ Bq year}^{-1} / 4132 \text{ m}^3 \text{ year}^{-1} = 1.3 \text{ mBq m}^{-3}$$

Thus, activity concentrations in the environment of less than 1 mBq m⁻³ need to be quantifiable.

Main stack releases of ^{148}Gd

From the Gaussian plume modelling presented above, the momentary normalized ground level concentration, $\frac{c}{Q}$, for releases from the main stack is up to (see Figure 4):

$$\frac{c}{Q} = 1.4 \cdot 10^{-5} \text{ Bq m}^{-3} \text{ per Bq s}^{-1}$$

The maximum allowed average release rate Q from then main stack would then be:

$$Q = \frac{c(^{148}\text{Gd})}{c/Q} = \frac{1.3 \text{ mBq m}^{-3}}{1.4 \cdot 10^{-5} \text{ Bq m}^{-3} \text{ per Bq s}^{-1}} = 93 \text{ Bq s}^{-1}$$

Waste stack releases of ^{148}Gd

Using the same assumption as for the main stack, the maximum allowed releases of ^{148}Gd can be estimated for the waste stack. For the waste stack, the momentary normalized ground level concentration, $\frac{c}{Q}$, is up to (see Figure 5):

$$\frac{c}{Q} = 4 \cdot 10^{-5} \text{ Bq m}^{-3} \text{ per Bq s}^{-1}$$

The maximum allowed average release rate Q from then waste stack would then be:

$$Q = \frac{c(^{148}\text{Gd})}{c/Q} = \frac{1.3 \text{ mBq m}^{-3}}{4 \cdot 10^{-5} \text{ Bq m}^{-3} \text{ per Bq s}^{-1}} = 32 \text{ Bq s}^{-1}$$

Releases of W

The amount of W released in particulate form is also of interest to assess the loading of W on filters used in aerosol samplers. The thickness of W on the filter will strongly affect the energy straggling and stopping of alpha particles emitted in the collected material on the filter. Knowing that each W brick (density 19.3 g cm^{-3}) in the ESS target has a volume of $(1.0 \cdot 3.0 \cdot 8.0) \text{ cm}^3$, and that the target has 36 sectors with 186 bricks in each sector (see [53] and references therein), the total mass of W in the target, $m(W)$, is estimated to be:

$$m(W) = 36 \cdot 186 \cdot (1.0 \cdot 3.0 \cdot 8.0) \text{ cm}^3 \cdot 19.3 \text{ g cm}^{-3} = 2.3 \cdot 10^3 \text{ kg}$$

If after 5 years of operation, the target inventory of ^{148}Gd is estimated to be $I(^{148}\text{Gd}) = 9.3 \cdot 10^{12} \text{ Bq}$ [53]. The ratio between the mass of W and the activity of ^{148}Gd in the target is thus:

$$\frac{m(W)}{I(^{148}\text{Gd})} = \frac{2.3 \cdot 10^3 \text{ kg}}{9.3 \cdot 10^{12} \text{ Bq}} = 2.4 \cdot 10^{-10} \text{ kg of W per Bq } ^{148}\text{Gd}$$

Assuming that the releases of W is proportional to the releases of ^{148}Gd , the maximum mass concentration of W in air, $C_{mass}(W)$, will thus be:

$$\begin{aligned} C_{mass}(W) &= \frac{m(W)}{I(^{148}\text{Gd})} \cdot C(^{148}\text{Gd}) = \\ &(2.4 \cdot 10^{-10} \text{ kg W per Bq } ^{148}\text{Gd}) \cdot (1.3 \text{ mBq m}^{-3}) = \\ &3.1 \cdot 10^{-13} \text{ kg W m}^{-3} = 3.1 \cdot 10^{-4} \text{ } \mu\text{g m}^{-3} \end{aligned}$$

As stated above, the annual average concentration of PM₁₀ in rural areas in southern Sweden is typically about 10 µg m⁻³ [6]. That is, under the condition that one would detect activity concentration levels of ¹⁴⁸Gd around the maximum permissible inhalation dose, and given the assumptions of proportionality between W and Gd-release, the contribution from W (or W oxides) to sampled mass of aerosols will be insignificant.

5.2. Alpha spectra from the rural reference site Hyltemossa

Since the HiVol aerosols samplers that will be used at the ESS during operation of the facility are not commissioned yet, another HiVol sampler (DHA-80, Digitec) was used to investigate the direct alpha spectrometry on aerosol filters from a rural background station. The sampler used is located at the ICOS/Actris³ site Hyltemossa (56°06'N, 13°25'E, 115 m asl), located 46 km NNE of Lund. The sampler is located on top of a roof of a building at the research station, which is surrounded by forest (see Figure 6). The DHA-80 sampler (with automatic filter change of up to 15 filters) is situated at the roof top of a building at Hyltemossa and has a maximum flow rate of 1000 L min⁻¹.



Figure 6 *Left:* The DHA-80 sampler on the roof of the Hyltemossa site. *Right:* Interior of the DHA-80 sampler, showing the filters mounted on filter holders.

Previously reported gamma spectrometric measurements using this sampler to collect aerosols at Hyltemossa used quartz fibre filters of 150 mm diameter (Advantec QR-100) (see chapter 5.2 in [42]). For alpha spectrometry, however, membrane filters are recommended (see e.g. [33]). Circular filters (diameter 15 cm) were cut out from membrane filter sheets (PALLFLEX membrane filters, type EMFABTX40HI20-WW⁴). Filters were weighed prior to being transported

³ ICOS: Integrated Carbon Observation System, <https://www.icos-ri.eu/>; ACTRIS: the European Research Infrastructure for the observation of Aerosol, Clouds, and Trace gases, <https://www.actris.eu/>

⁴ Size 8 x 10; Borosilicate glass microfibers reinforced with woven glass cloth and bonded with PTFE; Typical thickness: 178 µm; Typical filter weight: 5 mg cm⁻²; Typical aerosol retention following ASTM D 2986-95A 0.3 µm (DOP) at 32 L min⁻¹ per 100 cm² filter media: 99.95%.

to Hyltemossa and mounted on filter holders. The exposed filter area was 154 cm^2 (exposed filter diameter 14 cm). The flow rate of the time of sampling was 600 L min^{-1} and a PM10 inlet was used on the DHA-80 sampler. Sampling was conducted between 18 March and 1 June in 2022 and sampling intervals varied between <1 day and 3.5 days.

Figure 7 shows membrane filters with aerosols collected during 24 and 16 hours, respectively, with a flow rate of $\sim 36 \text{ m}^3 \text{ h}^{-1}$ using the DHA-80 HiVol sampler at Hyltemossa research station (see [42] for further details).



Figure 7 Aerosol-laden filter collected with a HiVol DHA-80 sampler (Digitel) at Hyltemossa research station with a flow rate of $\sim 36 \text{ m}^3 \text{ h}^{-1}$ (see [42] for further details). The filter diameter is 15 cm of which 14 cm is exposed (filter 3 in

Table 5 to the left and filter 2-11 to the right).

Filters were removed from the DHA sampler at various times, wrapped in aluminium foil, labelled and transported to Lund/Malmö for weighing and analysis. In total 26 filters were used for sampling, and a few were subjected to alpha spectrometry (see

Table 5). The rest of the filters are kept stored for possible future analysis (wrapped in Al foil and placed in plastic bags).

Table 5 PM10 samples collected on membrane filters at Hyltemossa research station using a flow rate about $0.6 \text{ m}^3 \text{ h}^{-1}$. * Uncertain values.

| No | Mass of unexposed filter (mg) | Mass of exposed filter (mg) | Collected aerosol mass (mg) | Surface density ($\mu\text{g cm}^{-2}$) | Start date | Stop date | Days of collection | Aerosol conc. ($\mu\text{g m}^{-3}$) |
|------|-------------------------------|-----------------------------|-----------------------------|---|------------------|------------------|--------------------|--|
| 1 | 938.0 | 943.1 | 5.1 | 33 | 2022-03-18 15:15 | 2022-03-19 15:15 | 1 | 5.9 |
| 2 | 918.0 | 923.7 | 5.7 | 37 | 2022-03-19 15:15 | 2022-03-20 15:15 | 1 | 6.6 |
| 3 | 937.9 | 952.2 | 14.3 | 93 | 2022-03-20 15:15 | 2022-03-21 15:15 | 1 | 16.6 |
| 4 | 930.3 | 948.0 | 17.7 | 115 | 2022-03-21 15:15 | 2022-03-22 15:15 | 1 | 20.5 |
| 5 | 941.0 | 961.0 | 20.0 | 130 | 2022-03-22 15:15 | 2022-03-23 15:15 | 1 | 23.1 |
| 6 | 924.5 | 943.4 | 18.9 | 123 | 2022-03-23 15:15 | 2022-03-24 12:33 | 0.9 | 24.6 |
| 7 | 937.6 | 990.7 | 53.1 | 345 | 2022-03-24 12:33 | 2022-03-28 03:19 | 3.5 | 17.6 |
| 8 | 929.3 | 952.2 | 22.9 | 149 | 2022-03-28 03:19 | 2022-03-31 15:19 | 3.5 | 7.6 |
| 9 | 933.5 | 945.3 | 11.8 | 77 | 2022-03-31 15:19 | 2022-04-04 03:19 | 3.5 | 3.9 |
| 10 | 925.9 | 939.8 | 13.9 | 90 | 2022-04-04 03:19 | 2022-04-07 15:19 | 3.5 | 4.6 |
| 11 | 925.9 | 949.3 | 23.4 | 152 | 2022-04-07 15:19 | 2022-04-11 03:19 | 3.5 | 7.7 |
| 12 | 941.0 | 973.0 | 32.0 | 208 | 2022-04-11 03:19 | 2022-04-14 15:19 | 3.5 | 10.6 |
| 13 | 939.5 | 952.0 | 12.5 | 81 | 2022-04-14 15:19 | 2022-04-18 03:19 | 3.5 | 4.1 |
| 14 | 932.5 | 947.4 | 14.9 | 97 | 2022-04-18 03:19 | 2022-04-21 15:19 | 3.5 | 4.9 |
| 15 | 939.5 | 955.6 | 16.1 | 105 | 2022-04-21 15:19 | 2022-04-25 03:19 | 3.5 | 5.3 |
| 2-1 | 927.2 | 947.3 | 20.1 | 131 | 2022-04-25 03:19 | 2022-05-01 06:34 | 2.6 | 8.9 |
| 2-2 | 927.1 | 949.6 | 22.5 | 146 | 2022-05-01 06:34 | 2022-05-04 18:34 | 3.5 | 7.4 |
| 2-3 | 935.7 | 965.1 | 29.4 | 191 | 2022-05-04 18:34 | 2022-05-08 06:34 | 3.5 | 9.7 |
| 2-4 | 931.1 | 981.2 | 50.1 | 325 | 2022-05-08 06:34 | 2022-05-11 18:34 | 3.5 | 16.6 |
| 2-5 | 932.4 | 984.6 | 52.2 | 339 | 2022-05-11 18:34 | 2022-05-15 06:34 | 3.5 | 17.3 |
| 2-6 | 932.1 | 957.8 | 25.7 | 167 | 2022-05-15 06:34 | 2022-05-18 18:34 | 3.5 | 8.5 |
| 2-7 | 936.2 | 963.0 | 26.8 | 174 | 2022-05-18 18:34 | 2022-05-22 06:34 | 3.5 | 8.9 |
| 2-8 | 933.6 | 954.5 | 20.9 | 136 | 2022-05-22 06:34 | 2022-05-25 18:34 | 3.5 | 6.9 |
| 2-9 | 936.6 | 952.9* | 16.3* | 106* | 2022-05-25 18:34 | 2022-05-29 06:34 | 3.5 | 5.4* |
| 2-10 | 935.9 | 941.9* | 6.0* | 39* | 2022-05-29 06:34 | 2022-05-31 21:19 | 2.6 | 2.6* |
| 2-11 | 936.9 | 939.5* | 2.6* | 17* | 2022-05-31 21:19 | 2022-06-01 13:35 | 0.7 | 4.4* |

The alpha spectrometry setup located at Medical Radiation Physics Malmö was used to perform measurements. The setup is composed of 8 PIPS detectors of 2 cm diameter active area placed in individual vacuum chambers (6 in an Alpha Ensemble and 2 in an Alpha Duo system, from Ortec). Vacuum is achieved with an oil pump. Detector 1 has 1000 channels while the others have 2000. The setup is controlled by a Maestro-32 software (Ortec). A picture of the setup is presented in Figure 8.



Figure 8 The alpha detector setup used for measurement of the membrane filters.

The energy calibration of the detectors and the determination of their efficiency was performed using an open ^{242}Pu and ^{243}Am source (DTU Risø, Denmark) with reference activities of 1.80 Bq and 1.78 Bq for Pu and Am, respectively. Samples were placed in contact with the edges of the detectors (approximately 2 mm from the active area). At this distance the detectors presented an efficiency of 38.6 to 40.6%. An example of calibration spectrum with the reference source is presented in Figure 9.

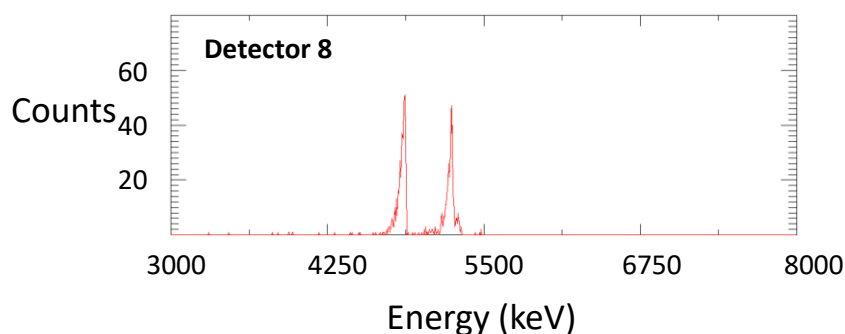


Figure 9 Example of energy calibration spectra obtained by sampling under vacuum in a PIPS chamber using the reference open Pu-Am source.

Background spectra were taken regularly to take into account the possible contamination of the detector or vacuum chambers. The backgrounds were typically measured over a few days on each detector and were found to be low (around 0.1 mBq for the largest peaks). Some contamination from radon daughters could be observed on some detectors but the counts per second from the most recently measured background were always subtracted from the filter measurements. Typical background measurements of some of the alpha chambers are shown in Figure 10.

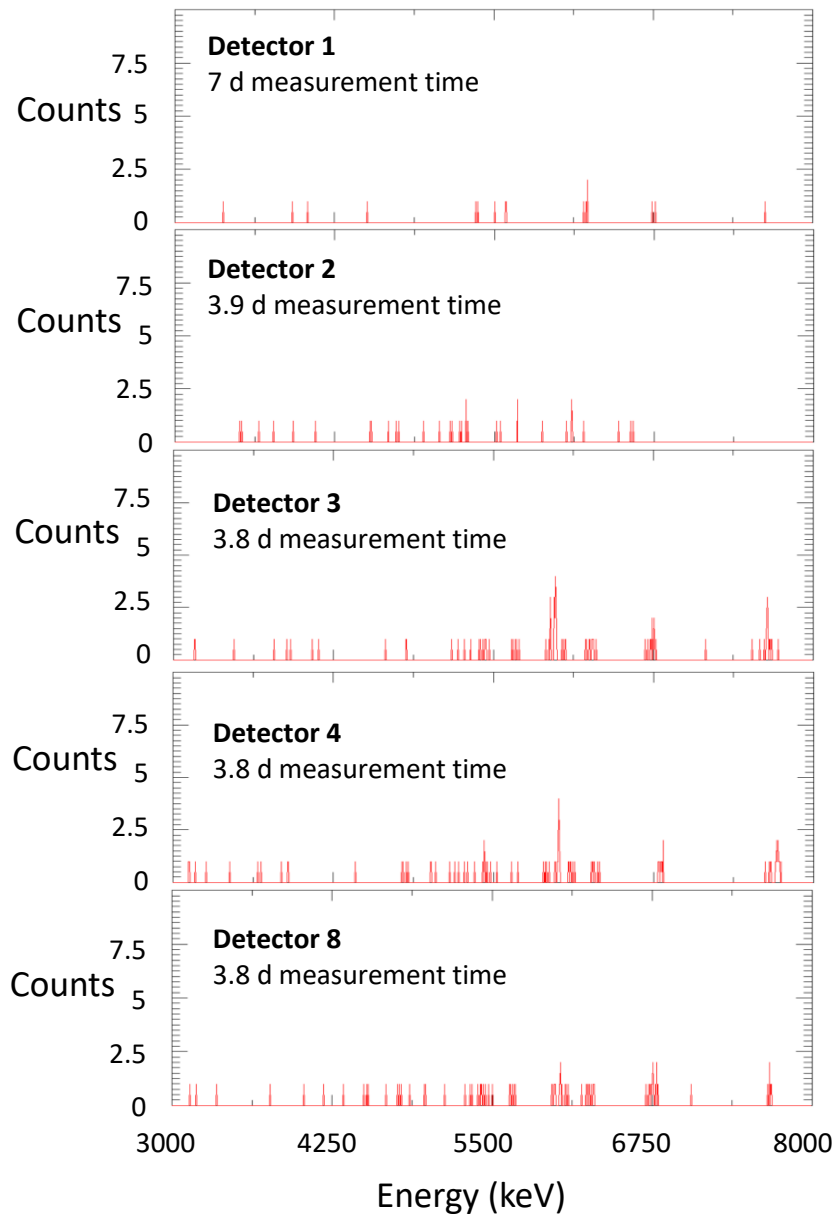


Figure 10 Detector background alpha spectra for some of the alpha chambers (measured in the end of May 2022).

Filter blanks wrapped in Al foil were placed inside the HiVol sampler for several months. Figure 11 shows examples of alpha energy measurements of these filter blanks, without and with subtraction of the detector backgrounds. The detector background is negligible compared to the filter blank measurements, demonstrating the importance of filter blank measurements in case of low-activity measurements.

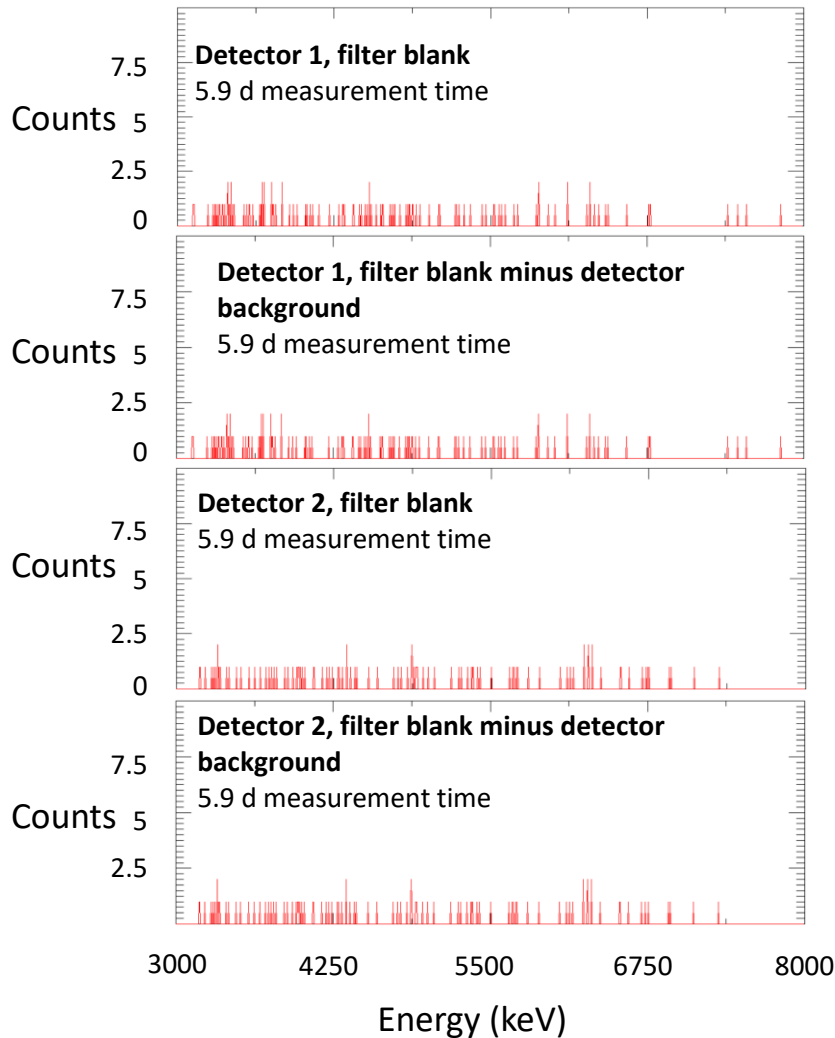


Figure 11 Alpha spectra of filter blanks and background-subtracted filter blanks for some of the alpha chambers (measured in the beginning of June 2022).

Figure 12 shows alpha spectra for the filter 2-11 (Table 5) at various times after start of data acquisition. Aerosols were sampled on this filter for 16 hours at Hyltemossa research station and the filter was then transported directly to the alpha spectrometry laboratory in Malmö. Data acquisition started about 2.5 hours after end of sampling. The spectra are as expected from radon progenies [30] (see also Appendix 2). The vast majority of the counts are collected within the first 17 hours of data acquisition. The broad peak at around 6000 keV (peak at 6025 keV) is attributed mainly to ^{212}Bi ($T_{1/2} = 60.55$ min; several alpha energies, mainly $E = 6051$ keV (25.1%), 6090 keV (9.8%)) and less to ^{218}Po ($T_{1/2} = 3.07$ min; $E = 6003$ keV (99.98%)). Significantly less contribution is

believed to arise from ^{214}Bi (5 alpha energies between 4941 keV and 5516 keV, branching ratios all $< 0.0113\%$) from the uranium series, and less likely ^{211}Bi ($T_{1/2} = 2.14$ m; $E_1 = 6623$ keV (83.54%), $E_2 = 6278$ keV (16.19%), $E_3 = 5299$ keV ($< 0.002\%$)) from the actinium series. The broad peak at higher energy results mainly from ^{214}Po ($T_{1/2} = 162$ μs , $E = 7687$ keV (99.99%)) and tails from ^{212}Po ($T_{1/2} = 0.3$ μs , $E = 8785$ keV). Coincidences may also have been recorded (see [30]). The broad peaks result from attenuation in the filter and in the aerosol sample itself.

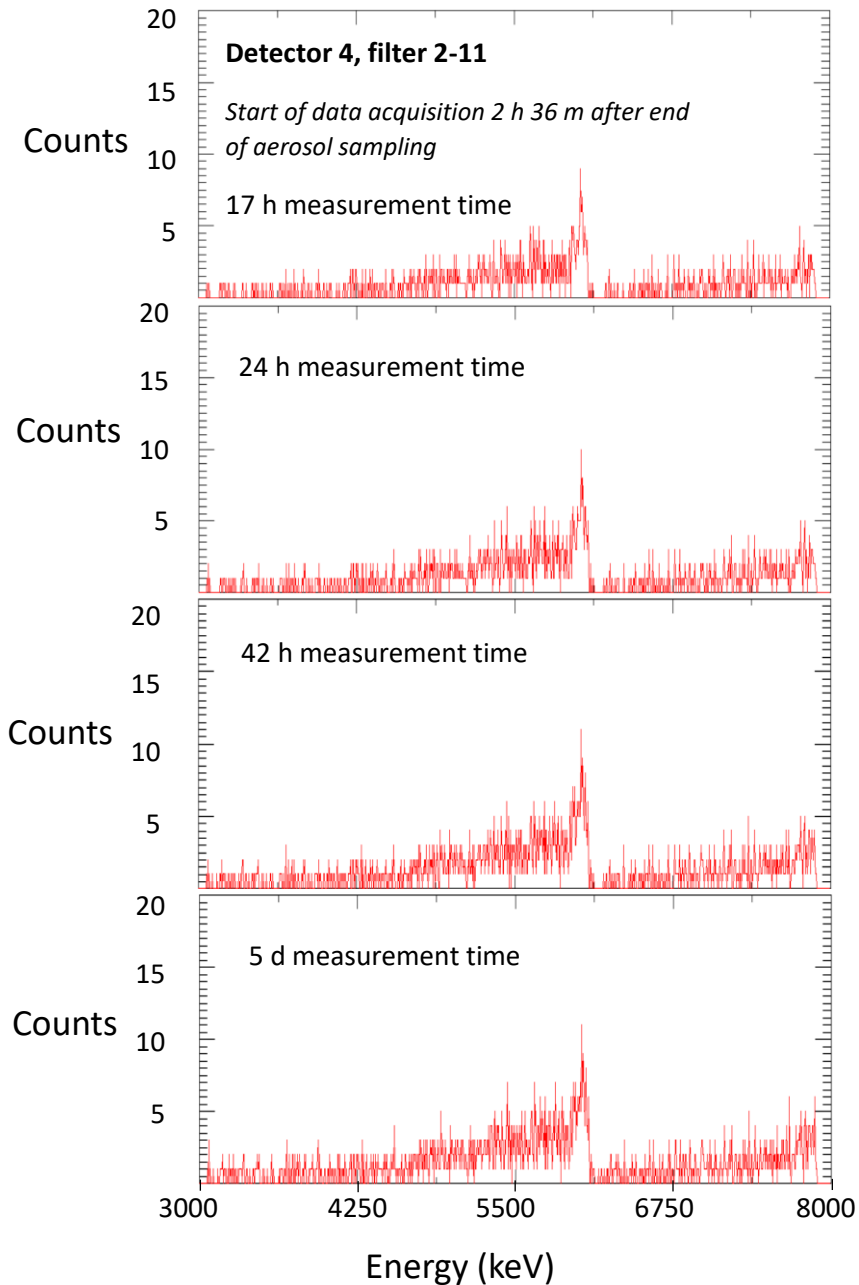


Figure 12 Alpha spectra from filter 2-11 collected at Hyltemossa research station (

Table 5). Data acquisition started 2 hours and 36 minutes after end of aerosol sampling. The time noted in the graphs is the total data acquisition time after start of the alpha measurement (2022-06-01 16:11). Aerosol surface density $\sim 17 \mu\text{g cm}^{-2}$. Spectra have not been background subtracted.

In Figure 13, alpha spectra collected during 42 h of two filters are presented, where the data acquisition started 19 h after end of aerosol collection for one of the filters and 4.3 days after end of aerosol sampling for the other filters (both filters had sampled aerosols for 3.5 days). As demonstrated in the graph, the radon progeny interference is very low if starting data collection several days after end of sampling.

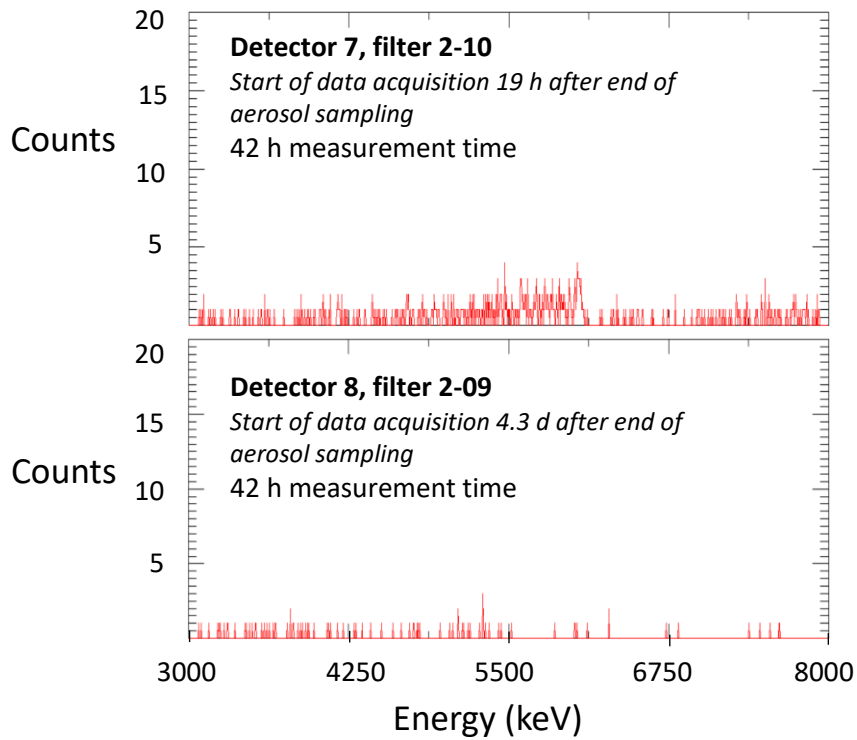


Figure 13 Alpha spectra from filter 2-10 and 2-09 (aerosol surface density 39 and $106 \mu\text{g cm}^{-2}$, respectively, see

Table 5) with data acquisition started 19 h and 2.3 days after end of aerosol sampling, respectively. The time is the total data acquisition time after start of the alpha measurement. Spectra not background subtracted.

Some of the aerosol-laden filters were measured several months after end of sampling, as shown in Figure 14 (two subsamples of filter 9 was measured, denoted 9A and 9B). Both filters in Figure 14 have been subjected to aerosol collection for 3.5 days. For the filters in Figure 14, almost all radionuclides preceding ^{210}Pb ($T_{1/2} = 22.2$ y) have decayed in the uranium series (see Appendix 1 and 2). The only relevant alpha decay (here defined as a branching ratio (BR) of $> 0.1\%$) from the uranium series is therefore ^{210}Po ($T_{1/2} = 138$ d, $E = 5304$ keV (100%)). The 5304 keV alpha from ^{210}Po corresponds to the peak at maximum intensity in all spectra in Figure 14. The branching ratios of alpha decay (BR_α) for ^{210}Pb and ^{210}Bi are very low ($< 10^{-4}\%$) and their contributions to the spectra are negligible. In the thorium series (see Appendix 1 and 2), the radionuclide with the longest half-life of the daughters to ^{220}Rn is ^{212}Bi ($T_{1/2} = 60.54$ min; several alpha energies, mainly $E_1 = 6061$ keV (25.1%) and $E_2 = 6090$ keV (9.8%)). The contribution of ^{212}Bi in the thorium series to the spectra in Figure 14 is considered negligible (more than 3000 half-lives have passed). The contributions from radon progenies in the actinium series are also deemed insignificant to the spectra in Figure 14: the most long-lived daughter to ^{219}Rn is the beta emitter ^{211}Pb ($T_{1/2} = 61$ min), which is followed by an alpha decay of ^{211}Bi ($T_{1/2} = 2.14$ m; $E_1 = 6623$ keV (83.54%), $E_2 = 6278$ keV (16.19%)). Additionally, radionuclides from the actinium series generally contribute less to natural radioactive aerosols, due to the lower natural abundance of ^{235}U compared to ^{238}U .

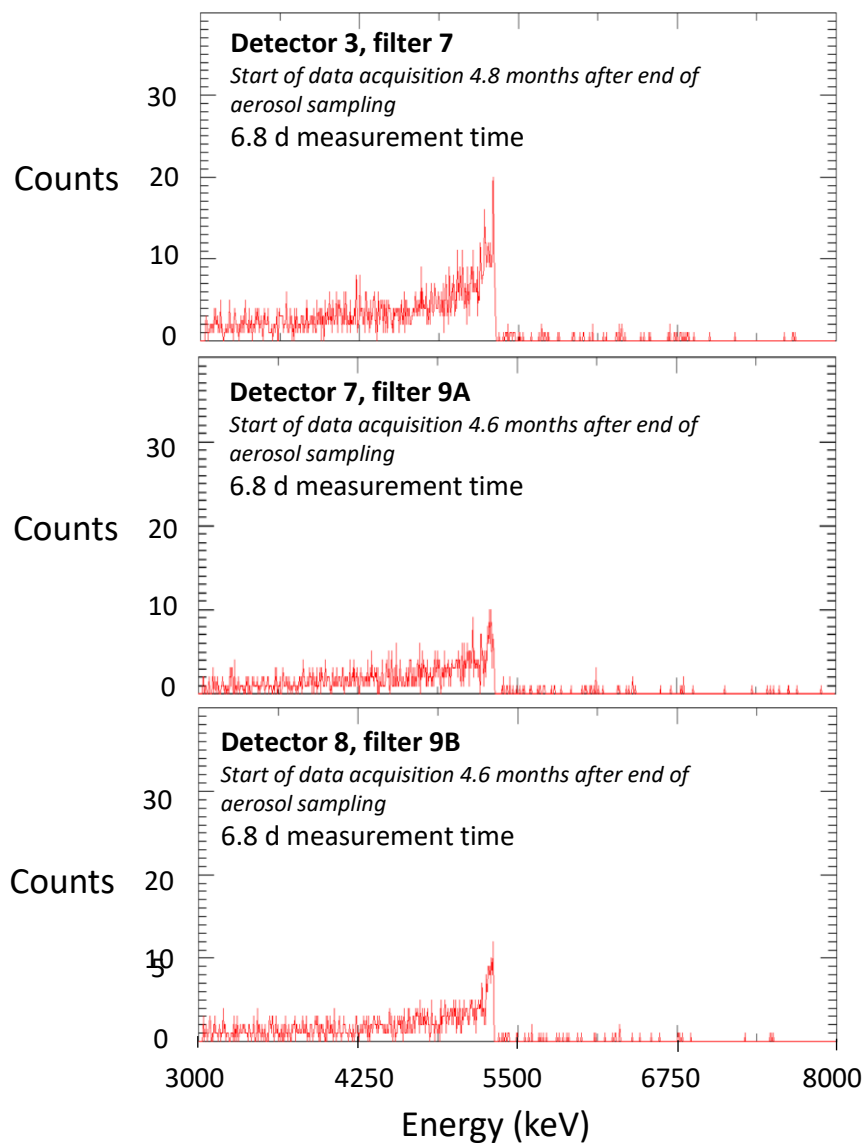


Figure 14 Alpha spectra from filter 7 and 9 (aerosol surface density 345 and 77 $\mu\text{g cm}^{-2}$, respectively, see

Table 5) with data acquisition started 4.8 to 4.6 months after end of aerosol sampling (3.5 days of aerosol sampling). The time is the total data acquisition time after start of the alpha measurement. The peak at ~5300 keV is attributed to ^{210}Po . The spectra have not been background subtracted.

For the filters in Figure 14, filter 7 has ~ 4.5 times the collected mass of aerosols compared filter 9 (aerosol surface densities 345 and $77 \mu\text{g cm}^{-2}$). A higher count rate is also observed in the spectrum of filter 7 compared to filter 9: the total count in the energy range 4660-5340 keV is 1361 counts for the sample for filter 7, and 708 counts and 666 counts for the each of the samples from filter 9 (i.e. a factor of 2). The same relationship applies to 3612-4660 keV (940, 442 and 468 counts for 7, 9B and 9A respectively). The higher count rate in filter 7 compared to filter 9 may be a result of higher outdoor radon concentrations at the time of sampling for filter 7 than for filter 9. A higher fraction of unattached aerosols (the unattached fraction increases with decreasing aerosol concentration [54]) may also play a role.

Figure 15 shows two filters where aerosols have been collected for 1 day (the filters in Figure 14 were sampled for 3.5 days), and where alpha spectra were acquired several months after sampling. Filter 1 has a low amount of sampled aerosol (aerosol surface density $33 \mu\text{g cm}^{-2}$), whereas filter 4 has approximately 4 times this mass (surface density $115 \mu\text{g cm}^{-2}$). As for the filters in Figure 14, different outdoor aerosol concentrations and unattached fractions may be influential.

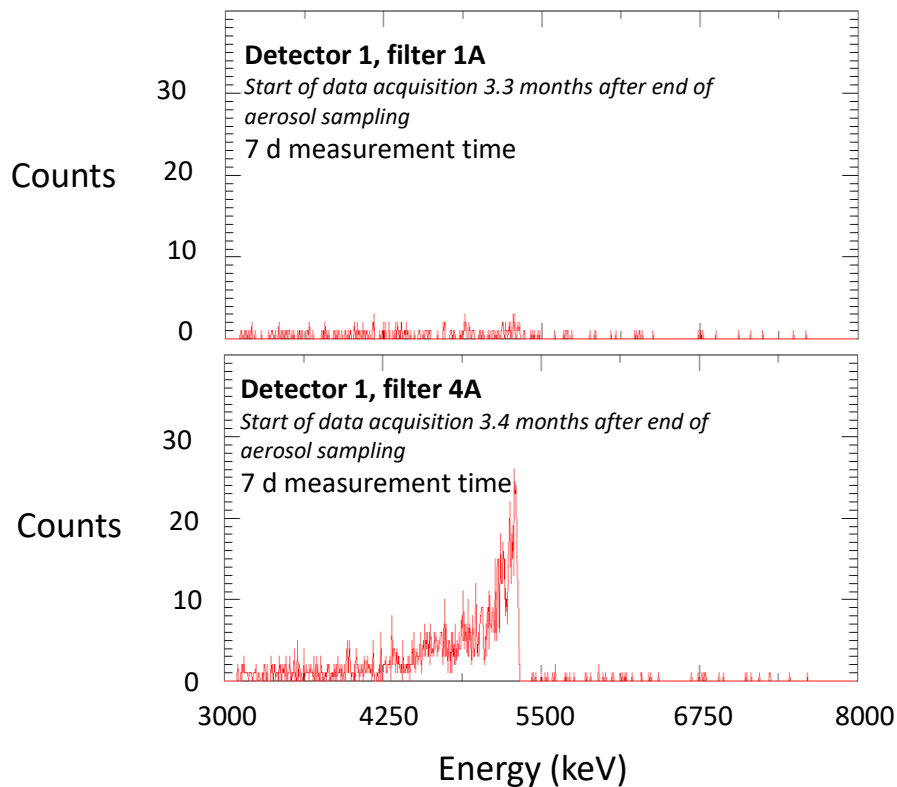


Figure 15 Alpha spectra from filter 1 and 4 (aerosol surface density 33 and $115 \mu\text{g cm}^{-2}$, respectively, see

Table 5) with data acquisition started 3.3 to 3.4 months after end of aerosol sampling (1 day of aerosol sampling). The time is the total data acquisition time after start of the alpha measurement. The peak at ~5300 keV is attributed to ^{210}Po . The spectra have not background subtracted.

Polonium-210 on atmospheric aerosols may not only originate from radon released from the ground to the atmosphere, but also from e.g. forest fires, fossil fuel combustion and coal-fired power plants [55]. The ^{210}Po activity on the filter with the highest ^{210}Po activity, filter 4 (Figure 16), was roughly estimated assuming no total self-absorption of alpha particles in the filters. The spectrum was stripped using the filter blank for detector 1 (see Figure 11, note that the filter blank may not be entirely representative to the sample due to different storage times and handling procedures). A total number of 1324 counts for ^{210}Po were collected the ROI (region of interest) 4200-5365 keV during 677 307 s, giving a count rate of $0.002 \text{ counts s}^{-1}$ and an activity of $\sim 2 \text{ mBq } ^{210}\text{Po}$. Using a detector efficiency of $\sim 40\%$, an active detector area of 3.1 cm^2 (2 cm diameter), and a total filter area of 154 cm^2 (exposed filter diameter 14 cm), the total ^{210}Po activity of the filter is estimated to 0.24 Bq. The time of aerosol sampling was 24 h and the flow rate $\sim 36 \text{ m}^3 \text{ h}^{-1}$, giving a ^{210}Po activity concentration corresponding to 0.3 mBq m^{-3} . The division between ^{210}Po originating from progenies of radon released from the ground to the atmosphere (caught on the filter and decaying to ^{210}Po during the 3.4 months storage time), and ^{210}Po originating from other sources (such as forest fires and combustion of fossil fuels) is not known in the present study. The estimated ^{210}Po activity concentration in air is a reasonable value compared to other studies, showing a large wide range of concentrations [55]. The same procedure for filter 1, gives a ^{210}Po concentration in air of $\sim 0.02 \text{ mBq m}^{-3}$ (a very rough estimate), which is also within the range of reported values in the literature [55].

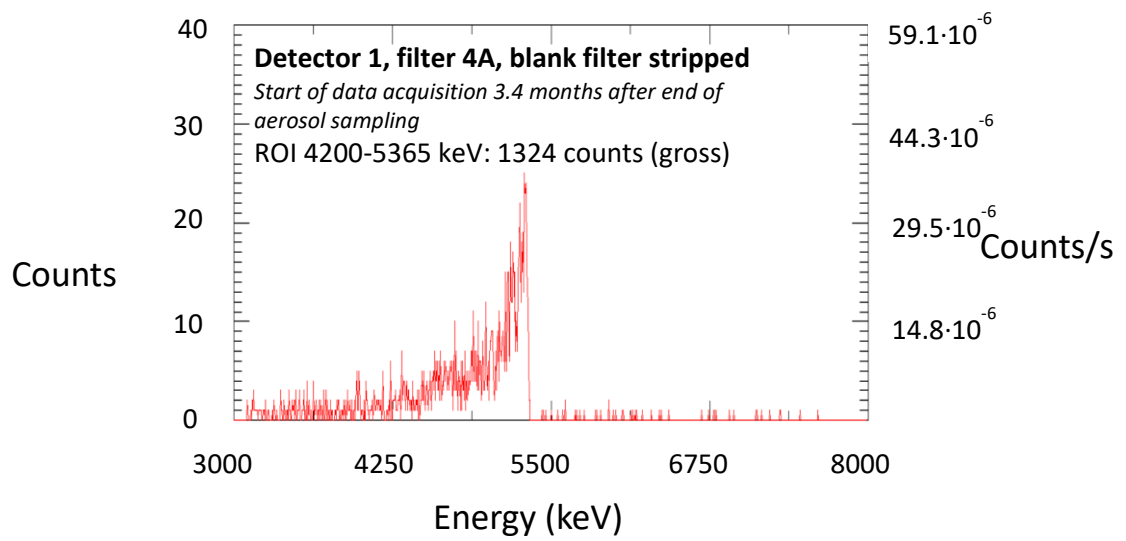


Figure 16 Alpha spectra from filter 4 (aerosol surface density $115 \mu\text{g cm}^{-2}$, see

Table 5) with data acquisition started 3.4 months after end of aerosol sampling (1 day of aerosol sampling). The time is the total data acquisition time after start of the alpha measurement. The peak at 5298 keV is attributed to ^{210}Po (5304 keV in theory). The spectrum has been background subtracted using a filter blank for detector 1 (see Figure 11).

Risk of detector contamination

Some contamination of the alpha detectors by radon daughters was observed after the measurement of aerosol laden membrane filters. Visible marks were also left by the samples on the holders with suggest releases on both sides of the filter. Most ^{222}Rn daughters are short-lived but the presence of longer-lived ^{210}Pb ($T_{1/2} = 22.3$ y) poses the risk of long-term and continuous production of alpha-emitting ^{210}Po on the contaminated surfaces.

This type of contamination was not observed on end filters of cascade impactor loaded with ^{210}Po in soot particles. This could be due to the fact that there were less particles on the filters or that there were more strongly bound to its surface.

Satisfactory counts can be obtained with shorter measurement times than the ones performed in this study. Limiting the time of measurement could decrease the risk of contamination. The distance between the detector and the filter could also be increased for the same purpose without degrading the quality of the measurements. We would recommend additional test on the membrane filters, in particular performing measurements at atmospheric pressure instead of vacuum to limit the releases of aerosol particles from the filter.

5.3. Simulation of aerosol spectra from normal operation

An attempt was made to use a simplified approach to simulate alpha spectra for the Hyltemossa filters reported on above, using the software AASI⁵. Filter 4 in Figure 16 (see also

⁵ AASI software (<https://www.stuk.fi/web/en/services/aasi-program-for-simulating-energy-spectra-in-alpha-spectrometry> from STUK, Finland)

Table 5) serves as an example. The aerosols on this filter were collected during 24 hours and alpha measurement was performed 3.4 months after end of aerosol sampling. Aerosol surface density for this filter was approximately $115 \mu\text{g cm}^{-2}$. The alpha spectrum shows a ^{210}Po peak at 5298 keV, which is very close to the actual alpha energy of 5304 keV. The discrepancy between what the calibrated source predicts the position of the peak and the actual location in a sample will depend on the difference in the "penetration depth" between the source and the calibration source.

Basic input data needed in AASI relate to the source (the collected aerosols), the matrix (the filter) and the detector setup. The detector simulated is a PIPS300 detector (diameter 19.5 mm, FWHM 14.8 keV, dead layer thickness 0.05 μm , and thickness of active volume 100 μm). The filter (or source) was estimated to be at 2 mm from the detector, and in each simulation 3000 decays of ^{210}Po were used (if not stated otherwise).

5.3.1. Case 1: ^{210}Po in homogenous source of aerosols

In the first case, the ^{210}Po nuclei were assumed to be embedded in a layer of rural aerosols of varying thicknesses. Penetration of particles into the membrane filter was neglected. The elemental composition of the collected aerosols was roughly approximated from PM10 data in Northern Europe according Fuzzi et al [3] (see 2.2.3 in [3]) as 56% O, 17% N, 17% C and 8% S. Note that this approximation is very crude and neglects e.g. the influence of sea salt and mineral dust, as well as seasonal and other temporal variations.

The density of the aerosol particles was approximated to 2 g cm^{-3} [56]. The thickness of the aerosol layer of filter 4, if the particles were absorbed only on the surface of the filter would then be $115 \text{ } \mu\text{g cm}^{-2} / 2 \text{ g cm}^{-3} = 0.58 \text{ } \mu\text{m}$. Thicknesses of $0.01 \text{ } \mu\text{m}$, $0.5 \text{ } \mu\text{m}$, $1 \text{ } \mu\text{m}$, $5 \text{ } \mu\text{m}$ and $10 \text{ } \mu\text{m}$ were used in the simulations. Thickness fluctuation was set to $0 \text{ } \mu\text{m}$ for simplicity. As can be seen in Figure 17, self-absorption resulted in widened peaks. The broadened peaks for thicknesses $> 1 \text{ } \mu\text{m}$ will severely aggravate the possibility to successfully perform direct alpha spectrometry of several radionuclides. A thickness of an aerosol layer of $1 \text{ } \mu\text{m}$ and a density of 2 g cm^{-3} corresponds to a surface density of $200 \text{ } \mu\text{g cm}^{-2}$. Several of the aerosol samples in

Table 5, that were collected for longer than 1 day, have higher surface densities than this. Hence, it can be concluded direct alpha spectrometry of aerosols collected on filters by HiVol samplers operating for several days will be unsuccessful. Alpha spectrometry after chemical extraction (see [57]) would however benefit from the high amounts of material collected.

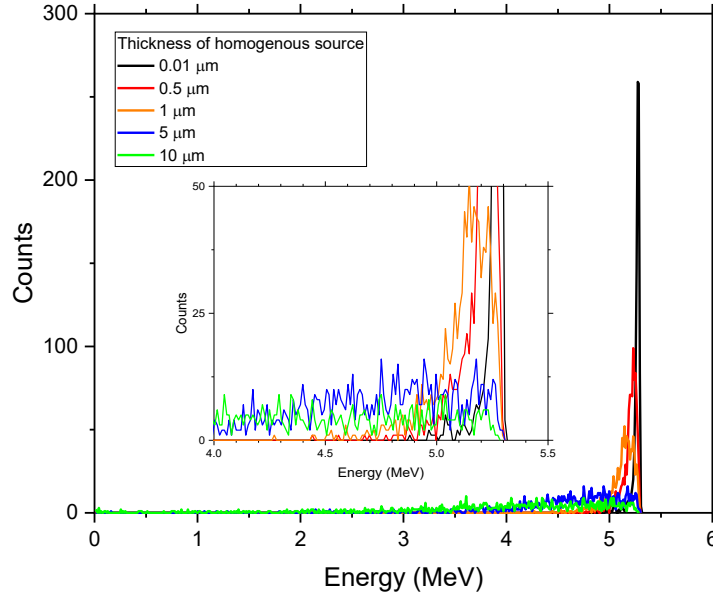


Figure 17 AASI simulations of alpha spectra of ^{210}Po in a homogenous source of aerosols (elemental composition 56% O, 17% N, 17% C and 8% S) of varying thicknesses.

5.3.2. Case 2: Radioactive particles in a homogenous source matrix

Case 1 excluded direct alpha spectrometry for aerosol layers with thicknesses of $> 1 \mu\text{m}$. Filter 4 in Figure 16 is thinner than this ($\sim 0.6 \mu\text{m}$ using a density of 2 g cm^{-3}). In case 2, the aerosols collected on Filter 4 were assumed to have penetrated into the membrane filter. The membrane filters used were made of borosilicate glass microfibers reinforced with woven glass cloth and bonded with PTFE, had a typical thickness of $178 \mu\text{m}$ and a typical filter weight of 5 mg cm^{-2} , and hence density of 0.281 g cm^{-3} . In the AASI simulations, the matrix (filter) elemental composition was therefore set as SiO_2 (main part of borosilicate glass). The thickness fluctuation was set to $8.9 \mu\text{m}$ (5%). The mean penetration depth was set to $100 \mu\text{m}$, to serve as an example. The percentage of particles to distribute exponentially was set to vary between 5%, 50% and 95%.

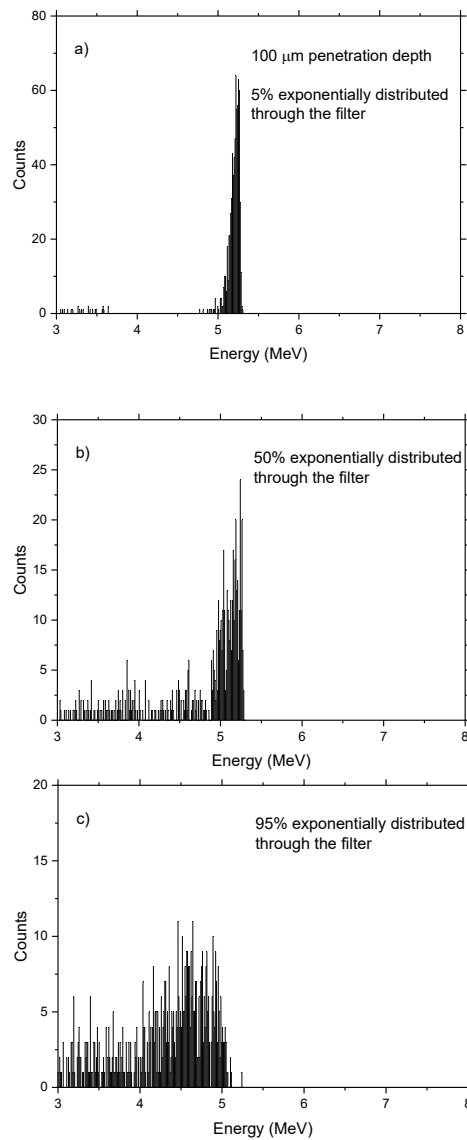


Figure 18 AASI simulation of alpha spectra for ^{210}Po deposited on a membrane filter with different degree of penetration into the filter matrix.

For the source (the collected aerosol particles), the options “Radioactive particles in a homogenous source matrix”, “Spherical particle size” and “Lognormally distributed particle size” were chosen in the AASI simulation. The “Diameter ceiling” (i.e. the maximum diameter of the particles) was set to $10\ \mu\text{m}$ since PM10 was collected. “Count mean diameter” (mean diameter of the particles in which the radioactive particles are embedded) was set to $0.5\ \mu\text{m}$ and geometrical standard deviation to 1.5. In this simulation, the effect of the filter is evaluated, and not the effect of self-absorption in the aerosol sample. The effect of energy loss through interactions of the alpha particles with the filter is demonstrated in Figure 18, with increasing energy losses and increased peak tails with increasing penetration depth.

5.3.3. Case 3: Effect of particle size

The particle size in which the radioactive particle is embedded also affect the alpha spectra, which is illustrated in Figure 19. In this simulation, the average penetration depth has been set to 20 μm and 5% of the particles have been distributed exponentially into the membrane filter. Alpha spectra for particle sizes of 0.5 μm , 2 μm and 10 μm were simulated. Large particles of 10 μm have extensive peak tailing.

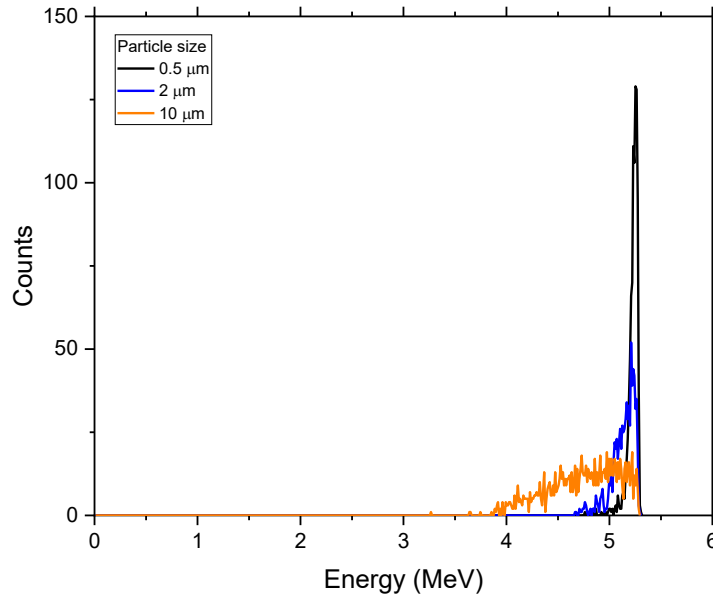


Figure 19 AASI simulation of alpha spectra for ^{210}Po deposited on a membrane filter with different particle size. 5% of the particles have been distributed exponentially into the filter and the mean penetration depth was set to 20 μm .

5.3.4. Comparison with measured spectrum

The shape and energy of the measured spectrum (Figure 16) can be compared with the simulated examples above. The low number of collected counts in the ^{210}Po peak in Figure 16 limits the comparison. The shape of the spectrum is most likely a combination of the parameters presented in three cases above.

5.3.5. Notes on suitable aerosol sampling flow rates

The previous section estimated that the surface density of collected aerosols needs to be less than $\sim 200 \mu\text{g cm}^{-2}$ for direct alpha spectrometry. The maximum flowrate of a specific aerosol sampling device collecting PM10 during a given time can be estimated from this number. For example, if collecting aerosols for 1 week, and assuming an average aerosol concentration of maximum $40 \mu\text{g m}^{-3}$, the maximum flow rate should not exceed $4.6 \text{ m}^3 \text{ h}^{-1}$ (76 L min^{-1}) if using filters of 14 cm in diameter.

The ESS will purchase several high-volume iodine and aerosol samplers from ALGADE INSTRUMENTATION of the model EAS 100K. The majority of the samplers will be placed in at the ESS site in different wind directions from the ventilation stacks of the main building and the waste building. Sampling flowrates will be adjustable from 60 to 90 m³ h⁻¹. The samplers have the possibility to be equipped with an impactor for measurement of size-distributed aerosols. In EAS 100K, aerosols are sampled on filters for off-line analysis. Supported filter types are paper filters, fibreglass and polypropylene. The sampling period can be up to one week. The diameter of the filters is 128 mm and filter area 129 cm². Assuming a flow rate of 75 m³ h⁻¹ the aerosol sampling rate on the filter will typically be 750 µg h⁻¹ for PM10 and 1.5 mg h⁻¹ for TSP (now assuming a PM10 concentration of 10 µg m⁻³ [6] and TSP concentration twice as high as the PM10 concentration [7]). One day of sampling would typically collect 18 mg PM10 and 37 mg TSP, and for one week of sampling the corresponding values are 126 mg and 252 mg for PM10 and TSP, respectively. The corresponding surface density for one week of sampling will thus be (126 mg) / (129 cm²) = 0.98 mg cm⁻² for PM10 and (252 mg) / (129 cm²) = 1.95 mg cm⁻² for TSP. Therefore, filters from these samplers will not be useful for direct alpha spectrometry due to the high aerosol load on the filters.

5.3.6. Hypothetical alpha spectrum from normal operation of the ESS

Assuming that an aerosol collection system provides filters with an aerosol surface density of less than 200 µg cm⁻² (76 L min⁻¹ if using filters of 14 cm in diameter for a collection period of 1 week), and that the concentration of ¹⁴⁸Gd is 1.3 mBq m⁻³ (see section 5.1.2), the total activity on the filter would be 1.0 Bq after 1 week of aerosol collection. Assuming further that there is no complete self-absorption in the filter or in the sample itself. Taking the detector efficiency and reduced area of the filter measured into account, the count rate in the detector would be 0.008 counts s⁻¹ (i.e. ~4 times higher than the count rate of ²¹⁰Po in the ROI 4200-5365 keV in filter 4 above). The energy of the alpha particles in the ¹⁴⁸Gd decay is 3182.7 keV. Count rates at this energy with a ROI of ~600 keV energy width can be estimated to be less than 0.00008 counts s⁻¹ (based on the filters in Figure 13, measured within a few days after end of aerosol sampling, containing ~40 and ~110 µg cm⁻²). These estimates are very rough but indicate a signal to background ratio of about 100 for the maximum allowed average activity concentration.

Other alpha emitters of ESS origin may also be present in the filter, but as discussed in the next section, ¹⁴⁸Gd is believed to be dominating and has significantly longer half-life than the rest (after 1 week, ¹⁴⁸Gd will dominate completely). Figure 20 shows a simulation of ¹⁴⁸Gd added to a 0.6 µm thick homogenous source of ²¹⁰Po in aerosols (compare with Figure 17). Acquisition time is set to 3 days (same detector setup as in Figure 17). The two peaks are clearly separated. However, real spectra will have more pronounced peak tailing (compare with Figure 16), along with possible coincidences interferences from other decay types. Additionally, in case of accidental releases from the ESS target, tungsten oxides may also be present in the aerosol samples, which will result in further broadening of the peaks. This is further discussed in the next session.

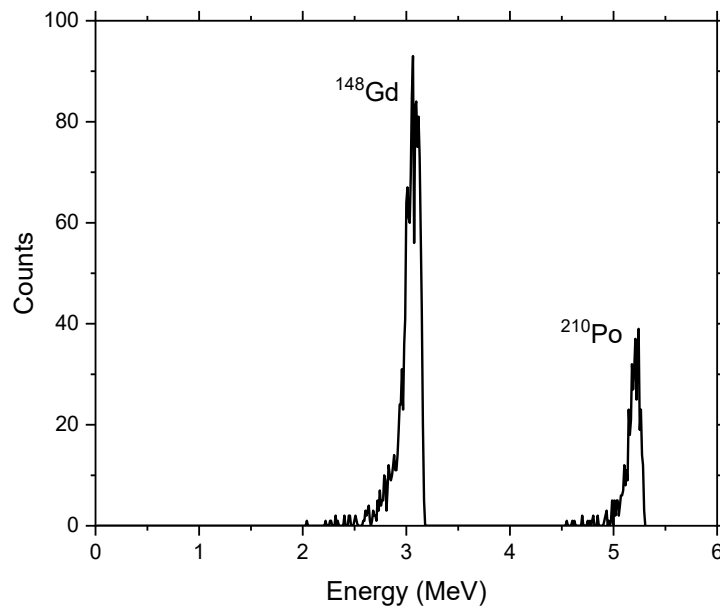


Figure 20 AASI simulations of alpha spectra of ^{210}Po and ^{148}Gd in a homogenous source of aerosols (elemental composition 56% O, 17% N, 17% C and 8% S), using an acquisition time of 3 days.

5.4. Conclusions

The main conclusion of the tests from the Hyltemossa filters and from the AASI simulations is that for direct alpha spectrometry the samples need to be thin (surface density less than $\sim 200 \mu\text{g cm}^{-2}$), but still provide enough registered decays within a reasonable measuring time (a few days). Another important aspect is that the size of the aerosols in which the radioactive particles are embedded is a critical parameter in the resulting alpha energy spectra: smaller aerosol sizes give more distinct spectra. This fact, in combination with the high dosimetric dependence on aerosol size, implies that size fractionated sampling would be beneficial. Impaction systems for size fractionation of sampled aerosols should therefore be considered.

Alpha spectrometry of filters covered with aerosols collected from outdoor air at Hyltemossa research station demonstrates that short-lived radon progenies should be allowed to decay for a few days prior to alpha measurement if the main goal is to assess the presence of low concentrations the more long-lived ^{148}Gd . Filters analysed long time (months) after collection show the presence of ^{210}Po . The energy of the main alpha peak from ^{210}Po (5304 keV) is however significantly higher than that of ^{148}Gd (3183 keV), and in a theoretical energy spectrum containing only these two radionuclides, the peaks are easily separated given that the thickness of the aerosol layer is thin (surface density less than $\sim 200 \mu\text{g cm}^{-2}$), that the particle size is small ($\ll 1 \mu\text{m}$) and that the penetration of particles into the filter is small.

6. Aerosol alpha spectra during an accident scenario

Releases of alpha emitting aerosols from the ESS during a worst-case accident scenario are presented in this chapter. Estimates are made on potential activities of alpha emitters in aerosols collected on filters and measured with direct alpha spectrometry after various filter storage times. The effect on alpha energy spectra from released tungsten oxide aerosols deposited on the filters is considered. A few different scenarios of fundamental energy spectra resulting from using various sampling flow rates and filter areas are presented. A simplified approach is used in the simulations of the alpha spectra, not considering probable interferences from other radiation types registered in the alpha detector.

6.1. The AA3 accident scenario

The accident scenario AA3, used by SSM to classify the ESS facility as a threat category II facility [1], is based on the IAEA classification of nuclear or radiation-related facilities [58]. For threat category II facilities, on-site events are not expected to give rise to doses leading to severe deterministic health effects to people off the site but may still warrant urgent protective action.

In the AA3 scenario, described in [1], target wheel cooling is lost during beam on target. Security systems are set to be non-operational. Four release phases occur [1, 59]:

- 1) **Target He-cooling loop break.** When the helium cooling stops working properly, the casing of the W target breaks after 100 s due to the heat and the He gas and filter particles escape. In total, 30 kg of He (100% of the He coolant) and 10 g of filter particles (41% of the filter particles) are released during 10 s.
- 2) **Slow release of W and Be from target and lower reflector.** The melted target casing causes leaks in the water moderator. Moderator water leaks into the target and is evaporated, which oxidizes the W target. The target stops rotating at 200 s due to the deposited heat and the oxidation. After another 10 s, two W target sections melt (those exposed to the proton beam). In total 50.3 kg of W is oxidized and melted. 41% of the melted and oxidized W (20.7 kg of W) and radionuclides therein are expected to be released for 17 minutes (starting at 100 s). The remaining 29.6 kg of W will be deposited in the target area. According to the TOAST experiments [60], W is expected to be released as WO₂ and WO₃. The melted W causes Be in the lower reflector to melt (15.7 kg). 100% of the noble gases and ³H, 10% of the semi volatile and 1% of the less volatile nuclides are expected to be released.

- 3) **Moderator water release.** Starting after 100 s, radionuclides dissolved in the boiling moderator water will be released (44% of the 400 kg of available water will be released up to 10 000 s).
- 4) **Hydrogen deflagration.** After 5 000 s, hydrogen deflagration will during 10 s release 0.5% of the 29.6 kg previously deposited W in the target area (i.e., 0.15 kg of W will be released).

The releases from the melted and oxidized tungsten target (phase 2) will dominate the effective dose [1]. The ESS document ESS-0095522 presents the amount of activity of the various radionuclides that are expected to be released during the different phases of the AA3 event [61]. Alpha emitting radionuclides have been extracted to Table 6, excluding phase 3 (moderator water release: alpha activity released $< 10^{-48}$ Bq).

The most important radionuclides for the first 7 days after a major accident are estimated to be ^{148}Gd , ^{187}W , ^{172}Hf , ^{182}Ta and $^{178\text{n}}\text{Hf}$, with the first one having the highest dosimetric impact [1]. Ref [1] also states that for the dimensioning accident scenario at the ESS, the main part of the effective dose during the first 7 days will be dominated by the inhalation dose, followed by groundshine and cloudshine. Inhalation dose of ^{148}Gd is of highest importance as it may contribute more than 50% to the total effective dose. Being a pure alpha emitter, ^{148}Gd only contributes to the effective dose from inhalation, whereas cloudshine and groundshine will be insignificant for this radionuclide.

Since the purpose of the aforementioned study was to dimension the general emergency preparedness zones and IAEA threat category classification [1], classification of absorption types has been done based on conservative dose estimates. For class F particulates, the dose coefficients for 1 μm AMAD size are typically 20% higher than for 5 μm AMAD size, whereas for class M types the dose coefficients are generally 40% lower than for 5 μm AMAD. Knowledge of the particle size is thus desirable and depending on the accident scenario, the size distribution of the dispersed particles is of great importance for the inhalation doses to workers and the general public.

The ESS consortium has performed a set of tests – the tungsten oxidation aerosol transport (TOAST) experiments [60] – to estimate the release of airborne tungsten oxides in air and steam at temperatures relevant for certain accident scenarios (temperature > 1400 °C). Primary particle size in case of low particle concentrations was estimated to be in the range of between 10 and 100 nm, while higher particle concentrations resulted in larger sizes due to agglomeration [60]. Particles transported through the whole experimental setup and sizes were in the order of 100-300 nm [60]. Agglomeration may however result in larger particle sizes for the inhaled fraction of workers and members of the public.

Table 6 Alpha emitters from the AA3 event [61]. Data for ¹⁴⁸Gd is in bold style.

| Nuclide | Z | Decay (BR%) | T _{1/2} | | Target He-cooling loop break | | | Slow W release from the target and Be release from reflector | | Hydrogen deflagration | |
|-----------------|-----------|-------------------------------------|---------------------|----------|------------------------------|------------------------|------------------------------|--|------------------------------|------------------------|------------------------------|
| | | | | | Energy alpha (keV) | Released activity (Bq) | Alpha activity released (Bq) | Released activity (Bq) | Alpha activity released (Bq) | Released activity (Bq) | Alpha activity released (Bq) |
| Pm-145 | 61 | α (2.8E-7%) EC (100%) | 17.7 6.80 | y | 2240 | 1.86E+06 | 5.21E-03 | 1.10E+11 | 3.08E+02 | 7.94E+08 | 2.22E+00 |
| Sm-146 | 62 | α (100%) α (0.0022%) | E+07 | y | 2460 | 0.00E+00 | 0.00E+00 | 3.12E+04 | 3.12E+04 | 2.25E+02 | 2.25E+02 |
| Eu-147 | 63 | EC (99.9978%) α (9.4E-7%) | 24.1 | d | 2908 | 9.39E+07 | 2.08E+01 | 1.21E+12 | 2.69E+05 | 8.67E+09 | 1.92E+03 |
| Eu-148 | 63 | EC β+ (100%) | 54.5 | d | 2630 | 1.09E+07 | 1.02E-01 | 1.53E+11 | 1.44E+03 | 1.10E+09 | 1.03E+01 |
| Gd-148 | 64 | α (100%) | 71.1 1.79 | y | 3182.69 | 2.43E+05 | 2.43E+05 | 3.48E+10 | 3.48E+10 | 2.50E+08 | 2.50E+08 |
| Gd-150 | 64 | α (100%) | E+06 | y | 2726 | 0.00E+00 | 0.00E+00 | 1.31E+06 | 1.31E+06 | 9.46E+03 | 9.46E+03 |
| Gd-151 | 64 | α (8E-7%) EC (100%) α (16.7%) | 123.9 | d | 2600 | 6.08E+07 | 4.86E-01 | 8.94E+11 | 7.15E+03 | 6.43E+09 | 5.14E+01 |
| Tb-149 | 65 | EC β+ (83.3%) α (0.022%) | 4.118 | h | 3967 | 1.67E+09 | 2.79E+08 | 8.11E+11 | 1.35E+11 | 4.60E+09 | 7.68E+08 |
| Tb-149m | 65 | EC β+ (99.978%) α (0.05%) | 4.16 | m | 3999 | 1.06E+09 | 2.33E+05 | 1.13E+11 | 2.49E+07 | 1.25E+03 | 2.75E-01 |
| Tb-150 | 65 | EC β+ (100%) α (0.0095%) | 3.48 | h | 3492 | 1.68E+09 | 8.40E+05 | 7.44E+11 | 3.72E+08 | 4.09E+09 | 2.05E+06 |
| Tb-151 | 65 | EC (99.9905%) α (0.0095%) | 17.6 | h | 3407 | 8.48E+08 | 8.06E+01 | 1.16E+12 | 1.10E+05 | 7.86E+09 | 7.47E+02 |
| Tb-151 | 65 | EC (99.9905%) α (36%) | 17.6 7.17 | h | 3183 | 8.48E+08 | 8.06E+04 | 1.16E+12 | 1.10E+08 | 7.86E+09 | 7.47E+05 |
| Dy-150 | 66 | EC β+ (64%) α (5.6%) | 6.4 3.00 | h | 4232 | 1.07E+09 | 3.85E+08 | 4.62E+11 | 1.66E+11 | 1.38E+06 | 4.97E+05 |
| Dy-151 | 66 | EC β+ (94.4%) α (0.1%) | 17.9 | m | 4069.4 | 1.10E+09 | 6.16E+07 | 6.56E+11 | 3.67E+10 | 2.00E+08 | 1.12E+07 |
| Dy-152 | 66 | EC β+ (99.9%) α (0.0094%) | 2.38 | h | 3628 | 1.07E+09 | 1.07E+06 | 1.18E+12 | 1.18E+09 | 5.60E+09 | 5.60E+06 |
| Dy-153 | 66 | β+ (99.9906%) | 6.4 3.00 | h | 3464 | 1.17E+12 | 1.10E+08 | 1.17E+12 | 1.10E+08 | 7.20E+09 | 6.77E+05 |
| Dy-154 | 66 | α (100%) α (12%) | E+06 1.62 | y | 2870 | 0.00E+00 | 0.00E+00 | 1.02E+06 | 1.02E+06 | 7.37E+03 | 7.37E+03 |
| Ho-152 | 67 | EC β+ (88%) α (0.0051%) | E+02 | s | 4386 | 5.61E+08 | 6.73E+07 | 1.31E+11 | 1.57E+10 | 9.89E-01 | 1.19E-01 |
| Ho-153 | 67 | EC β+ (99.949%) α (0.18%) | 2.01 | m | 3910 | 6.84E+08 | 3.49E+04 | 1.24E+11 | 6.32E+06 | 6.56E-04 | 3.35E-08 |
| Ho-153m | 67 | EC β+ (99.82%) α (0.019%) | 9.30 | m | 4011 | 2.91E+08 | 5.24E+05 | 1.40E+11 | 2.52E+08 | 2.51E+06 | 4.52E+03 |
| Ho-154 | 67 | EC β+ (99.981%) α (0.001%) | 11.8 | m | 3721 | 1.33E+09 | 2.53E+05 | 7.01E+11 | 1.33E+08 | 4.38E+07 | 8.32E+03 |
| Ho-154m | 67 | EC β+ (100%) α (0.47%) | 3.10 | m | 3721 | 2.30E+08 | 2.30E+03 | 6.21E+10 | 6.21E+05 | 1.60E+01 | 1.60E-04 |
| Er-154 | 68 | EC β+ (99.53%) α (0.022%) | 3.73 | m | 4168 | 6.99E+08 | 3.29E+06 | 2.06E+11 | 9.68E+08 | 4.02E+02 | 1.89E+00 |
| Er-155 | 68 | EC β+ (99.978%) | 5.30 | m | 4012 | 8.86E+08 | 1.95E+05 | 3.28E+11 | 7.22E+07 | 6.24E+04 | 1.37E+01 |
| SUM (Bq) | | | | | 1.18E+12 | 9.10E+08 | 1.15E+13 | 3.92E+11 | 5.47E+10 | 1.04E+09 | |

As mentioned previously, HiVol aerosol samplers used for environmental sampling are collecting aerosols on filters for a given time period (often up to 1 week). Laboratory-based alpha spectrometry of such aerosol-laden filters will not be carried out in a timeframe that enables measurement of the short-lived radionuclides with half-lives of seconds to minutes. Table 7 shows a simplified calculation (ingrowth not considered) of the ratio between individual released radionuclide alpha activity and total alpha activity released in the AA3 event as a function of time. ¹⁴⁸Gd (T_{1/2} 71.1 y) completely dominates the alpha activity on long-term basis, and also the effective dose [1]. For retrospective dose

assessments following an accident scenario, the most important information may thus be retrieved from aerosol filters measured even long time after the accident event (the longer time until measurement, the lower influence from short-lived alpha - and beta-emitters).

Table 7 Ratio between individual released radionuclide alpha activity and total alpha activity released in the AA3 event as a function of time [61]. ¹⁴⁸Gd dominates the alpha activity on long-term basis. Ingrowth is not considered.

| Nuclide | Fraction of total alpha activity | | | | |
|---------------------------|----------------------------------|------------------|------------------|------------------|------------------|
| | At release | After 6 h | After 1 day | After 3 days | After 1 week |
| Pm-145 | 7.870E-10 | 8.268E-09 | 8.268E-09 | 8.846E-09 | 8.845E-09 |
| Sm-146 | 7.972E-08 | 8.376E-07 | 8.376E-07 | 8.964E-07 | 8.967E-07 |
| Eu-147 | 6.864E-07 | 7.007E-06 | 7.007E-06 | 7.080E-06 | 6.312E-06 |
| Eu-148 | 3.675E-09 | 3.812E-08 | 3.812E-08 | 3.978E-08 | 3.781E-08 |
| Gd-148 | 8.892E-02 | 9.342E-01 | 9.342E-01 | 9.997E-01 | 9.999E-01 |
| Gd-150 | 3.347E-06 | 3.517E-05 | 3.517E-05 | 3.764E-05 | 3.765E-05 |
| Gd-151 | 1.828E-08 | 1.909E-07 | 1.909E-07 | 2.021E-07 | 1.977E-07 |
| Tb-149 | 3.462E-01 | 6.403E-02 | 6.403E-02 | 2.123E-05 | 2.039E-12 |
| Tb-149m | 6.366E-05 | 4.194E-108 | 4.194E-108 | 0 | 0 |
| Tb-150 | 9.510E-04 | 8.387E-05 | 8.387E-05 | 6.323E-09 | 3.139E-17 |
| Tb-151 | 2.817E-07 | 1.151E-06 | 1.151E-06 | 1.861E-07 | 4.254E-09 |
| Tb-151 | 2.817E-04 | 1.151E-03 | 1.151E-03 | 1.861E-04 | 4.254E-06 |
| Dy-150 | 4.229E-01 | 1.548E-60 | 1.548E-60 | 2.011E-181 | 0 |
| Dy-151 | 9.338E-02 | 5.953E-25 | 5.953E-25 | 2.346E-73 | 3.182E-170 |
| Dy-152 | 3.010E-03 | 2.914E-05 | 2.914E-05 | 2.647E-11 | 1.908E-23 |
| Dy-153 | 5.597E-04 | 4.371E-04 | 4.371E-04 | 2.584E-06 | 7.889E-11 |
| Dy-154 | 2.606E-06 | 2.738E-05 | 2.738E-05 | 2.931E-05 | 2.931E-05 |
| Ho-152 | 4.005E-02 | 7.521E-162 | 7.521E-162 | 0 | 0 |
| Ho-153 | 1.613E-05 | 3.680E-220 | 3.680E-220 | 0 | 0 |
| Ho-153m | 6.406E-04 | 1.648E-49 | 1.648E-49 | 1.057E-142 | 0 |
| Ho-154 | 3.385E-04 | 4.901E-40 | 4.901E-40 | 9.956E-114 | 3.589E-261 |
| Ho-154m | 1.581E-06 | 2.439E-145 | 2.439E-145 | 0 | 0 |
| Er-154 | 2.464E-03 | 1.577E-118 | 1.577E-118 | 0 | 0 |
| Er-155 | 1.836E-04 | 3.133E-85 | 3.133E-85 | 8.848E-249 | 0 |
| Total alpha activity (Bq) | 3.942E+11 | 3.752E+10 | 3.752E+10 | 3.506E+10 | 3.505E+10 |

Many of the short-lived radionuclides in target material has ¹⁴⁸Gd as decay product (e.g a series of positive beta decays / electron captures of isobars with mass number A = 148: ¹⁴⁸Tm → ¹⁴⁸Er → ¹⁴⁸Ho → ¹⁴⁸Dy → ¹⁴⁸Gd). The ingrowth of additional ¹⁴⁸Gd from these short-lived decays is however insignificant compared to the amount of originally released ¹⁴⁸Gd. Calculations for ingrowth from ¹⁴⁸Tm, ¹⁴⁸Er, ¹⁴⁸Ho, ¹⁴⁸Dy, ¹⁴⁸Tb, ^{148m}Tb, ¹⁵²Dy, ¹⁵⁶Er and ¹⁵²Ho [61] show that the total decay of these radionuclides would amount to about 1% of the number of ¹⁴⁸Gd originally released. Other alpha-emitters with

parents with half-lives of hours or more are ^{146}Sm , ^{150}Gd and ^{154}Dy : with time, their actual fraction of the total activity will be higher than the simplified calculations in Table 7 states. However, ^{148}Gd will still totally dominate among all alpha-emitters.

For direct alpha spectrometry on aerosol-laden filters, the stopping of alphas in other deposited material is of utmost importance for the resolution and quality of the energy spectrum. This material may be oxidized tungsten from the target but also aerosols from various natural and man-made sources. For high-sensitivity gamma spectrometry measurements, high flowrates are useful to obtain as much material as possible. As stated above, for alpha spectrometry measurements, thin samples are preferable due to the short range of alphas in matter. As reported above and further demonstrated below, aerosol-laden filters from HiVol samplers will not be suitable for direct alpha spectrometry, instead lower flowrates are needed.

6.2. Aerosol alpha spectra at the AA3 accident scenario

Three different scenarios are considered in this section using different flowrates for sampling of aerosols during the time of ongoing accidental releases. The following assumptions are made:

- The aerosol sampler is assumed to be located down-wind from the releases at a distance where the ground-level activity concentrations are the highest.
- Sampling starts at start of accident and ends at stop of the accident scenario (in total 17 min).
- The dispersion from the stack is assumed to be as during normal operation with the annual average wind speed and Pasquill stability class C (see Figure 4).
- The influence of tungsten oxides is taken into account, whereas normal background aerosols are neglected (see Scenario 1 below).
- Filters are not measured until the majority of the short-lived alphas have decayed (> 1 week after end of aerosol sampling), leaving only ^{148}Gd on in the alpha spectra.
- The AASI simulations are performed for a homogenous source (the influence from penetration into the filter is neglected).
- Interference from other radiation types on the alpha spectra are not considered.

The last assumption is particularly far from realistic and requires further investigations. However, the main focus of this exercise is to investigate how the flowrates of the aerosol sampling system will influence the overall possibility to do direct alpha spectrometry.

The main mass and the main radioactivity collected on the filters will stem from stage 2 in the AA3 accident scenario (slow release of W and Be from target and lower reflector):

- In total 20.7 kg of W and radionuclides therein are expected to be released for 17 minutes (starting at 100 s).
- Assuming that the tungsten is released as WO₃ (molar mass M(WO₃) = (0.184 + 3·0.016) kg mol⁻¹ = 0.232 kg mol⁻¹) [60], the total released mass of WO₃ will be 26.1 kg.
- The source term of WO₃ will be 26.1 kg/(17·60 s) = 0.026 kg s⁻¹.
- Applying a dilution factor of 1.2·10⁻⁵ kg m⁻³ per kg s⁻¹ (downwind distance of 560 m for Pasquill stability class C), the maximum downwind concentration of WO₃ will be 3.25·10⁻⁷ kg m⁻³ = 0.325 mg m⁻³.

Scenario 1. Alpha spectra from aerosols collected on filter using a HiVol sampler (ALGADE INSTRUMENTATION of the model EAS 100K) with a flow rate of 75 m³ h⁻¹

The sampler in this scenario is the type that will be used in environmental monitoring at ESS. If collecting aerosols of 75 m³ h⁻¹ (1.25 m³ min⁻¹), the amount of WO₃ collected on the filter during 17 minutes will be:

$$0.325 \text{ mg m}^{-3} \cdot 1.25 \text{ m}^3 \text{ min}^{-1} \cdot 17 \text{ min} = 6.9 \text{ mg.}$$

Assuming that aerosols from other sources contribute with 20 µg m⁻³, the deposited aerosols from other sources would be

$$20 \text{ µg m}^{-3} \cdot 1.25 \text{ m}^3 \text{ min}^{-1} \cdot 17 \text{ min} = 0.42 \text{ mg.}$$

These can be neglected since WO₃ will be much more abundant.

The bulk density of sampled WO₃ is assumed to be 1.2 g cm⁻³ (powder of diameter 3.3 µm) [62] (nanopowders <100 nm have bulk density of 1.5 g cm⁻³ and true density of 7.15 g cm⁻³)⁶. The thickness of sampled WO₃ will then be

$$(6.9 \text{ mg} / 129 \text{ cm}^2) / 1.2 \text{ g cm}^{-3} = 45 \text{ µm.}$$

(Note: it is not of importance which density is used, since the resulting thickness will also change. The number of electrons per unit area will still be the same, and it is with these that the alpha particles interact when travelling through the source material.)

The activity of ¹⁴⁸Gd on the filter will be (released amount of activity from Table 6):

$$(1.2 \cdot 10^{-5} \text{ Bq m}^{-3} \text{ per Bq s}^{-1}) \cdot 3.51 \cdot 10^{10} \text{ Bq} \cdot ((1.25 \text{ m}^3 \text{ min}^{-1}) / 60 \text{ s min}^{-1}) = 8800 \text{ Bq}$$

Assume that a punch with 2 cm diameter (3.14 cm²) is taken to alpha spectrometry, the resulting activity on the subsample will be:

$$(3.14 \text{ cm}^2 / 129 \text{ cm}^2) \cdot 8800 \text{ Bq} = 214 \text{ Bq}$$

Using an alpha spectrometry measurement time of 5 min (300 s), the number of decays of ¹⁴⁸Gd during the measurement time will be:

$$300 \text{ s} \cdot 214 \text{ Bq} = 64200 \text{ decays}$$

⁶ https://ssnano.com/inc/sdetail/tungsten_oxide_nanoparticles/293

The AASI simulation presented in Figure 21 (detector 2 mm from source) demonstrates that the thickness of the sample widens the peak tremendously. Some of the alpha particles are even prevented from reaching the detector (efficiency ~20% compared to normally ~40%).

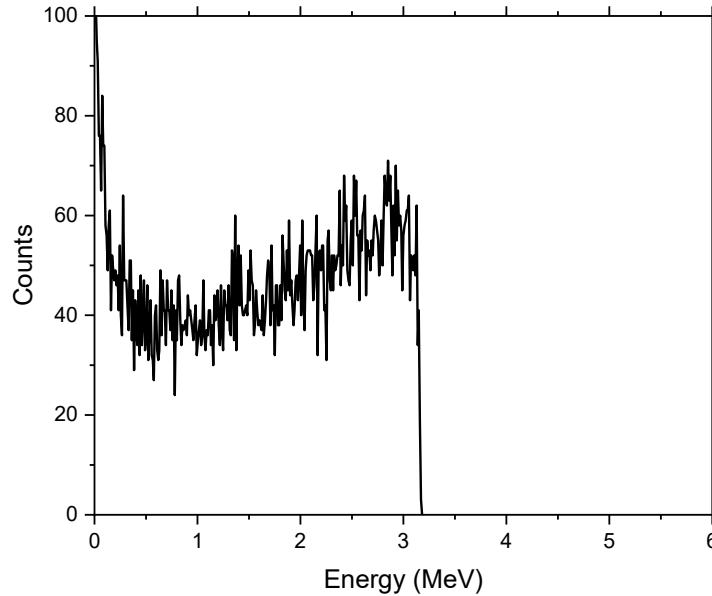


Figure 21 Homogenous source, 45 μm WO_3 (density 1.2 g cm^{-3}), 214 Bq, 5 min measurement time.

Scenario 2. Alpha spectra from aerosols collected on filter using a flow rate of 4.5 $\text{m}^3 \text{h}^{-1}$ during the accidental releases.

In this scenario the flow rate has been reduced to that recommended in section 5.3.6: an aerosol collection system providing filters with an aerosol surface density of less than 200 $\mu\text{g cm}^{-2}$, corresponding to 76 L min^{-1} (4.5 $\text{m}^3 \text{h}^{-1}$) if using filters of 14 cm in diameter for a collection period of 1 week).

Since the flow rate is reduced by a factor of 17 (75/4.3), the thickness and activity will be reduced by this factor, giving:

$$\text{Thickness: } 45 \mu\text{m} / 17 = 2.7 \mu\text{m}$$

$$\text{Activity on subfilter: } 214 \text{ Bq} / 17 = 13 \text{ Bq}$$

Using an alpha spectrometry measurement time of 1 hour (3 600 s), the number of decays of ^{148}Gd during the measurement time will be:

$$3\,600 \text{ s} \cdot 13 \text{ Bq} = 47\,000 \text{ decays}$$

The AASI simulation presented in Figure 22 (detector 2 mm from source) shows a significant improvement in peak shape compared to Scenario 1. Essentially no alpha particles are lost in the WO_3 source.

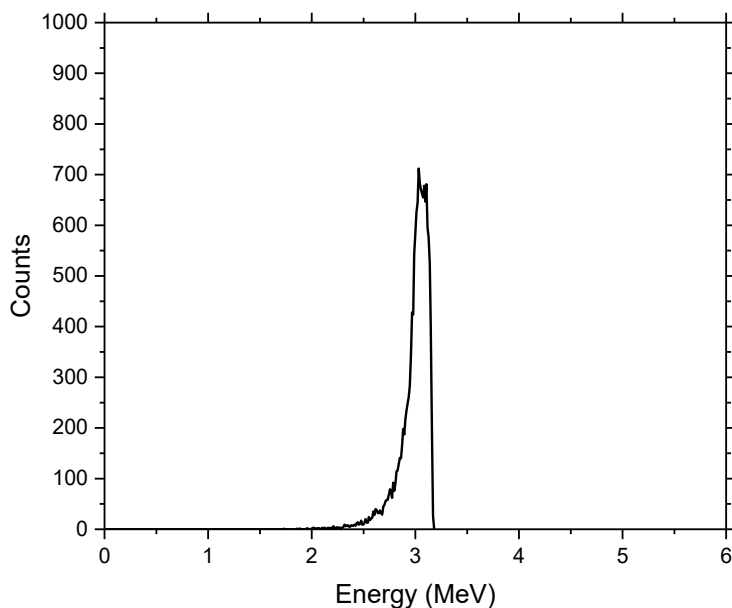


Figure 22 Homogenous source, 2.7 μm WO_3 (density 1.2 g cm^{-3}), 13 Bq, 1 hour measurement time.

Scenario 3. Alpha spectra from aerosols collected on filter using a flow rate of 2 L min^{-1}

The flow rate in this final scenario is what can be collected using a personal cascade impactor system, operating at 2 L min^{-1} (0.12 $\text{m}^3 \text{h}^{-1}$) and collecting particles in different size stages. The flow rate is reduced by a factor of 625 (75/0.12) compared to Scenario 1. The filter area in such systems is usually smaller than for HiVol samplers, and in this example the filter diameter is assumed to be 3.4 cm (filter area 9.1 cm^2). Compared to Scenario 1, the filter area is decreased by a factor 14 (129/9.1). The thickness of the sampled aerosol layer would then be reduced by a factor of 45 (625/14) compared to Scenario 1, assuming that all particles end up in the same impaction stage. The thickness of the aerosol layer would then be 1 μm (45 $\mu\text{m}/45$).

The activity of ^{148}Gd in the impaction stage in question will be:

$$(1.2 \cdot 10^{-5} \text{ Bq m}^{-3} \text{ per Bq s}^{-1}) \cdot 3.51 \cdot 10^{10} \text{ Bq} \cdot ((0.002 \text{ m}^3 \text{ min}^{-1}) / 60 \text{ s min}^{-1})) = 14 \text{ Bq}$$

Assume that a punch with 2 cm diameter (3.14 cm^2) is taken to alpha spectrometry, the resulting activity on the subsample will be:

$$(3.14 \text{ cm}^2 / 9.1 \text{ cm}^2) \cdot 14 \text{ Bq} = 5 \text{ Bq}$$

Using an alpha spectrometry measurement time of 1 hour (3 600 s), the number of decays of ^{148}Gd during the measurement time will be:

$$3\,600 \text{ s} \cdot 5 \text{ Bq} = 18\,000 \text{ decays}$$

The AASI simulation presented in Figure 23 (detector 2 mm from source) shows a further reduced peak width compared to the two previous scenarios.

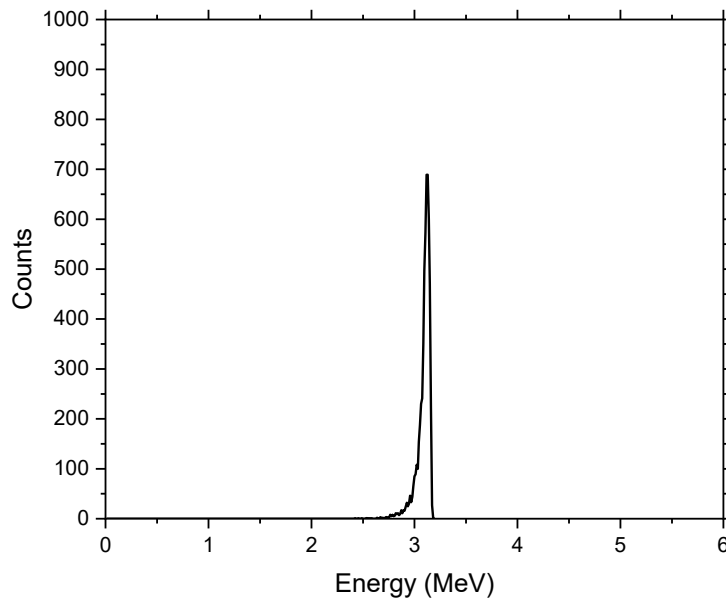


Figure 23 Homogenous source, $1 \mu\text{m WO}_3$ (density 1.2 g cm^{-3}), $5 \text{ Bq } ^{148}\text{Gd}$, 1 hour measurement time.

6.3. Conclusions

The main conclusion is that direct alpha spectrometry on aerosol filters obtained from HiVol samples will not be successful in case of an accident scenario. The release of tungsten oxides in aerosol will result in samples that will suffer from severe self-absorption of alphas. Aerosol collection systems using lower flow rates may avoid self-absorption issues.

The alpha activity in aerosols collected on filters at an accident scenario will be totally dominated by ^{148}Gd if the filters are not measured until several days after end of aerosol sampling. The interferences from other types of radiation have not been considered in this project, but need to be before assessing if direct alpha spectrometry is feasible for aerosols collected at an accident scenario.

7. Summary and conclusions

Measurements as well as simulations have shown that HiVol samplers operating at flowrates of several 10s of $\text{m}^3 \text{h}^{-1}$ will not produce aerosol-laden filters that are suitable for direct alpha spectrometry. Convenient sampling periods for such HiVol samplers are in the order of 1 week which will produce aerosol layers that are too thick for direct alpha spectrometry, but excellent for gamma spectrometric analyses. This applies to normal operational releases as well as to an accident scenario. Chemical extraction methods will be needed for subsamples of such filters prior to alpha spectrometry.

Aerosol sampling systems using lower flow rates (single $\text{m}^3 \text{h}^{-1}$ or less) may possibly have success in providing suitable filters for direct alpha spectrometry. Simulations show that samplers that provide, within a given sampling period (typically 1 week during normal operation), an aerosol surface density of less than $\sim 200 \mu\text{g cm}^{-2}$ on membrane filters may produce alpha spectra with acceptable peak shape. This aerosol surface density will not be exceeded e.g. using a sampler with a PM10 inlet, filters of 14 cm in diameter and a flow rate of $\sim 4 \text{m}^3 \text{h}^{-1}$ (given that the average PM10 concentration does not exceed the annual legislative limit of $40 \mu\text{g m}^{-3}$). During normal operating conditions, activity concentrations of ^{148}Gd of significantly less than 1.3mBq m^{-3} air must be measurable to demonstrate compliance with dose limits. Simplified simulations and measurements of filters with aerosols collected at a rural background demonstrate that such ^{148}Gd activity concentrations may be measurable, given that the alpha spectrometric measurement is performed several days after end of aerosol sampling. However, the simplified calculations do not include possible (and probable) interference from other radiation types than alpha particles, nor coincidences. Further work on this topic is suggested as a next step towards deeming if direct alpha spectrometry for aerosol samples from the ESS is feasible.

Another factor that is crucial for successful direct alpha spectrometry is that the aerosol size, in which the radioactive particle is embedded, is not too large (preferably $< \text{single } \mu\text{m}$). The smaller the aerosol, the less peak tailing and self-absorption. This fact, in combination with the high dosimetric dependence on aerosol size, implies that size fractionated sampling would be beneficial. We suggest that future studies should investigate the use of impaction systems for size fractionation in the sampling of the aerosols. Further estimates and investigations of the probable size of ^{148}Gd -containing aerosols generated at different conditions at the ESS are also needed to evaluate the potential of direct alpha spectrometry.

At a potential severe accident at the ESS, large amounts of oxidized target material may be dispersed into surrounding air. Direct alpha spectrometry of aerosols collected on filters will then be further complicated not only due to the presence of high activities of numerous different radionuclides, but also due to presence of stable tungsten oxides. The excess concentration of aerosols containing tungsten oxides may result in too thick samples for successful direct alpha spectrometry. However, if exposed filters are removed directly after the

accident, low flow rate systems (single $\text{m}^3 \text{h}^{-1}$ or less) may have a sufficiently thin layer of aerosol. Direct alpha spectrometry of short-lived radionuclides will most probably be impossible, but if filter samples are stored for prolonged times prior to alpha spectrometry, the situation may be more favourable to quantify ^{148}Gd . Again, the size of the aerosol to which ^{148}Gd is attached is of utmost importance for the potential success of the direct alpha spectrometry measurement as well as for the dosimetry of potentially exposed individuals. This further motivates the use of size fractionated aerosol sampling as well as further studies on probable size distributions of radioactive aerosols generated from the ESS target during various types of possible accidental releases.

Many questions are remaining about the feasibility of direct alpha spectrometry for aerosols samples collected in ambient air outside the ESS facility. However, we believe that the huge potential gain in omitting the laborious and expensive chemical extraction prior to alpha spectrometry clearly motivates further efforts towards the development of direct alpha spectrometry of thin aerosol samples.

8. Acknowledgement

This study was financed by the Swedish Radiation Safety Authority SSM (SSM2021-787).

9. References

1. Blixt Buhr, A.M., Johansson, J., Kock, P., Karlsson, S., Lindgren, J., Tengborn, E. *Underlag till beredningsplaneringen kring ESS*. SSM2018:02. 2018.
2. Lanz, V., Prévôt, A., Alfarra, M., Weimer, S., Mohr, C., DeCarlo, P., Gianini, M., et al. *Characterization of aerosol chemical composition with aerosol mass spectrometry in Central Europe: an overview*. Atmospheric Chemistry and Physics, 10(21): 10453-10471, 2010.
3. Fuzzi, S., Baltensperger, U., Carslaw, K., Decesari, S., Denier van der Gon, H., Facchini, M.C., Fowler, D., et al. *Particulate matter, air quality and climate: lessons learned and future needs*. Atmospheric Chemistry and Physics, 15(14): 8217-8299, 2015.
4. Goossens, J., Jonckheere, A.-C., Dupont, L.J., Bullens, D.M. *Air pollution and the airways: lessons from a century of human urbanization*. Atmosphere, 12(7): 898, 2021.
5. IAEA. *IAEA safety glossary. Terminology used in nuclear safety and radiation protection. 2018 edition*. IAEA Publication 1830. 2019.
6. Ketzler, M., Wählin, P., Kristensson, A., Swietlicki, E., Berkowicz, R., Nielsen, O., Palmgren, F. *Particle size distribution and particle mass measurements at urban, near-city and rural level in the Copenhagen area and Southern Sweden*. Atmospheric Chemistry and Physics, 4(1): 281-292, 2004.
7. Kim, K.-H., Kim, M.-Y. *The effects of Asian dust on particulate matter fractionation in Seoul, Korea during spring 2001*. Chemosphere, 51(8): 707-721, 2003.
8. Brook, J.R., Dann, T.F., Burnett, R.T. *The relationship among TSP, PM10, PM2.5, and inorganic constituents of atmospheric particulate matter at multiple Canadian locations*. JAPCA-the Journal of the Air and Waste Management Association, 47(1): 2-19, 1997.
9. Genberg, J., Hyder, M., Stenström, K., Bergström, R., Simpson, D., Fors, E.O., Jönsson, J.Å., et al. *Source apportionment of carbonaceous aerosol in southern Sweden*. Atmospheric Chemistry and Physics, 11(22): 11387-11400, 2011.
10. Martinsson, J., Abdul Azeem, H., Sporre, M.K., Bergström, R., Ahlberg, E., Öström, E., Kristensson, A., et al. *Carbonaceous aerosol source apportionment using the Aethalometer model – evaluation by radiocarbon and levoglucosan analysis at a rural background site in southern Sweden*. Atmospheric Chemistry and Physics, 17(6): 4265-4281, 2017.
11. Yttri, K.E., Simpson, D., Nøjgaard, J.K., Kristensen, K., Genberg, J., Stenström, K., Swietlicki, E., et al. *Source apportionment of the summer time carbonaceous aerosol at Nordic rural background sites*. Atmospheric Chemistry and Physics, 11(24): 13339-13357, 2011.
12. Glasius, M., Hansen, A.M.K., Claeys, M., Henzing, J.S., Jedynska, A.D., Kasper-Giebl, A., Kistler, M., et al. *Composition and sources of carbonaceous aerosols in Northern Europe during winter*. Atmospheric Environment, 173: 127-141, 2018.
13. Ćeliković, I., Pantelić, G., Vukanac, I., Krneta Nikolić, J., Živanović, M., Cinelli, G., Gruber, V., et al. *Outdoor radon as a tool to estimate radon priority areas—a literature overview*. International Journal of Environmental Research and Public Health, 19(2): 662, 2022.
14. Paquet, F., Etherington, G., Bailey, M.R., Leggett, R.W., Lipsztein, J., Bolch, W., Eckerman, K.F., et al. *ICRP Publication 130: Occupational*

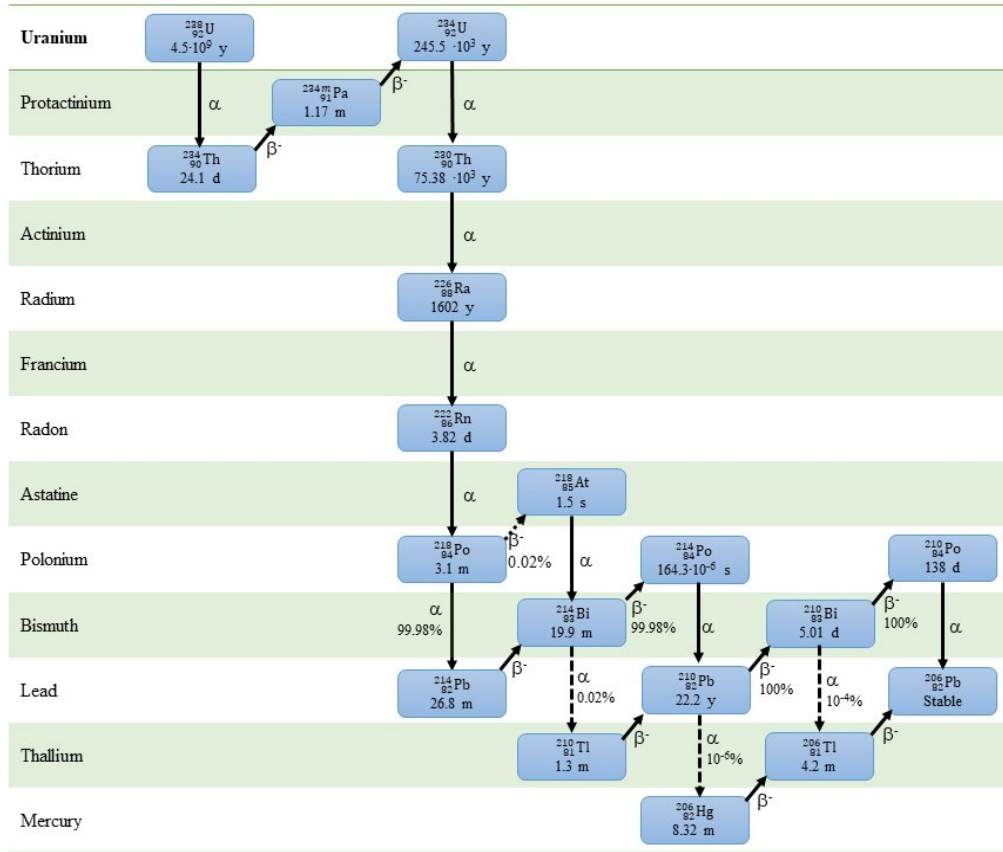
- intakes of radionuclides: Part 1*. Annals of the ICRP, 44(2): 5-188, 2015.
15. ICRP. *Human respiratory tract model for radiological protection*. ICRP Publication 66. Annals of the ICRP, 24 (1-3), 1994.
 16. ICRP. *ICRP supporting guidance 3. Guide for the practical application of the ICRP human respiratory tract model*. 2002.
 17. Rääf, C., Barkauskas, V., Eriksson Stenström, K., Bernhardsson, C., Pettersson, H.B.L. *Internal dose assessment of ^{148}Gd using isotope ratios of gamma-emitting ^{146}Gd or ^{153}Gd in accidentally released spallation target particles*. Scientific Reports, 10(1): 21887, 2020.
 18. ICRP. *Occupational intakes of radionuclides: Part 4*. ICRP Publication 141. Annals of the ICRP, 48(2-3), 2019.
 19. Maiello, M.L., Hoover, M.D., *Radioactive air sampling methods*. CRC press. 1420009680, 2010.
 20. Papastefanou, C. *Aerosol sampling and measurement techniques*. Radioactivity in the Environment, 12: 113-159, 2008.
 21. Papastefanou, C. *Chapter 11 - Radioactive aerosol analysis*, in *Handbook of Radioactivity Analysis (Third Edition)*, M.F. L'Annunziata, Editor. 2012, Academic Press: Amsterdam. p. 727-767.
 22. Hansson, E., Pettersson, H.B., Eriksson, M. *Uranium aerosol activity size distributions at a nuclear fuel fabrication plant*. Health Physics, 119(3): 327, 2020.
 23. Hansson, E., Pettersson, H.B., Yusuf, I., Roos, P., Lindahl, P., Eriksson, M. *Particle size-dependent dissolution of uranium aerosols in simulated lung fluid: A case study in a nuclear fuel fabrication plant*. Health Physics, 123(1): 11-27, 2022.
 24. Hansson, E., Pettersson, H., Fortin, C., Eriksson, M. *Uranium aerosols at a nuclear fuel fabrication plant: Characterization using scanning electron microscopy and energy dispersive X-ray spectroscopy*. Spectrochimica Acta Part B: Atomic Spectroscopy, 131: 130-137, 2017.
 25. International Atomic Energy Agency (IAEA). *Radioactive particles in the environment: sources, particle characterization and analytical techniques*. IAEA-TECDOC-1663. International Atomic Energy Agency (IAEA), Vienna. 2011.
 26. Baeza, A., Rodríguez-Perulero, A., Guillén, J. *Anthropogenic and naturally occurring radionuclide content in near surface air in Cáceres (Spain)*. Journal of Environmental Radioactivity, 165: 24-31, 2016.
 27. Pöllänen, R., Siiskonen, T. *High-resolution alpha spectrometry under field conditions – fast identification of alpha particle emitting radionuclides from air samples*. Journal of Environmental Radioactivity, 87(3): 279-288, 2006.
 28. Pöllänen, R., Peräjärvi, K., Siiskonen, T., Turunen, J. *In-situ alpha spectrometry from air filters at ambient air pressure*. Radiation Measurements, 53: 65-70, 2013.
 29. Ören, Ü., Nilsson, J., Herrnsdorf, L., Rääf, C.L., Mattsson, S. *Silicon diode as an alpha particle detector and spectrometer for direct field measurements*. Radiation protection dosimetry, 170(1-4): 247-251, 2016.
 30. Pöllänen, R., Siiskonen, T. *Unfolding alpha-particle energy spectrum from a membrane air filter containing radon progeny*. Radiation Measurements, 70: 15-20, 2014.
 31. Pöllänen, R., Siiskonen, T. *Direct high-resolution alpha spectrometry from nuclear fuel particles in an outdoor air sample*. Radiation protection dosimetry, 128(4): 454-463, 2008.

32. Pöllänen, R., Siiskonen, T. *Minimum detectable activity concentration in direct alpha spectrometry from outdoor air samples: continuous monitoring versus separate sampling and counting*. Health Physics, 90(2): 167-175, 2006.
33. Pöllänen, R., Siiskonen, T. *High-resolution alpha spectrometry under field conditions—fast identification of alpha particle emitting radionuclides from air samples*. Journal of Environmental Radioactivity, 87(3): 279-288, 2006.
34. Pöllänen, R., Peräjärvi, K., Siiskonen, T., Turunen, J. *High-resolution alpha spectrometry at ambient air pressure—Towards new applications*. Nuclear Instruments and Methods in Physics Research Section A: Accelerators, Spectrometers, Detectors and Associated Equipment, 694: 173-178, 2012.
35. Pöllänen, R. *Performance of an in-situ alpha spectrometer*. Applied Radiation and Isotopes, 109: 193-197, 2016.
36. Geryes, T., Monsanglant-Louvet, C., Gehin, E. *Experimental and simulation methods to evaluate the alpha self-absorption factors for radioactive aerosol fiber filters*. Radiation Measurements, 44(9): 763-765, 2009.
37. Pripachkin, D.A., Aron, D.V., Budyka, A.K., Khusein, Y.N. *Collimator Effect on Semiconductor α -Spectrometer Characteristics in Measurements of Radioactive Aerosols*. Atomic Energy, 125(2): 119-123, 2018.
38. Slade, D.H., *Meteorology and atomic energy, 1968*. U.S. Atomic Energy Commission, Division of Technical Information; [available from Clearinghouse for Federal Scientific and Technical Information, National Bureau of Standards, U.S. Department of Commerce, Springfield, Va.]. 1968.
39. Cember, H., Johnson, T.E., *Introduction to health physics*. The McGraw-Hill Companies, Inc. ISBN: 978-0-07-164323-8, 2009.
40. Isaksson, M., Rääf, C.L., *Environmental radioactivity and emergency preparedness*. CRC Press. ISBN: 978-1-4822-4464-9, 2017.
41. Ene, D. *Assessment of environmental consequences of the normal operations of ESS facility. Part #1 Input data Source Term. Breakdown of radionuclides & Related basic information*. ESS-0028551. 2016.
42. Eriksson Stenström, K., Barkauskas, V., Pedehontaa-Hiaa, G., Nilsson, C., Rääf, C., Holstein, H., Mattsson, S., et al. *Identifying radiologically important ESS-specific radionuclides and relevant detection methods*. SSM report of project SSM 2018-1636. <https://www.stralsakerhetsmyndigheten.se/publikationer/rapporter/stralskydd/2020/202008/>. 2020.
43. Bernhardsson, C., Eriksson Stenström, K., Pedehontaa-Hiaa, G., Jönsson, M. *Radiological environmental monitoring at the ESS facility – Annual report 2019*. Report MA RADFYS 2020:03, Report BAR-2020/03. 2020.
44. Eriksson Stenström, K., Skog, G., Bernhardsson, C., Mattsson, S., Nielsen, A.B., Rundgren, M., Muscheler, R., et al. *Environmental levels of radiocarbon in Lund, Sweden, prior to the start of the European Spallation Source*. Radiocarbon, 64(1): 51-67, 2022.
45. ESS. *Parameter data for radionuclide transport and dose calculations models for ESS*. ESS-0092831. 2017.
46. Endo, A., Oki, Y., Kanda, Y., Kondo, K. *Characterization of ^{11}C , ^{13}N and ^{15}O produced in air through nuclear spallation reactions by high energy protons*. Proceedings of 10th International Congress of the

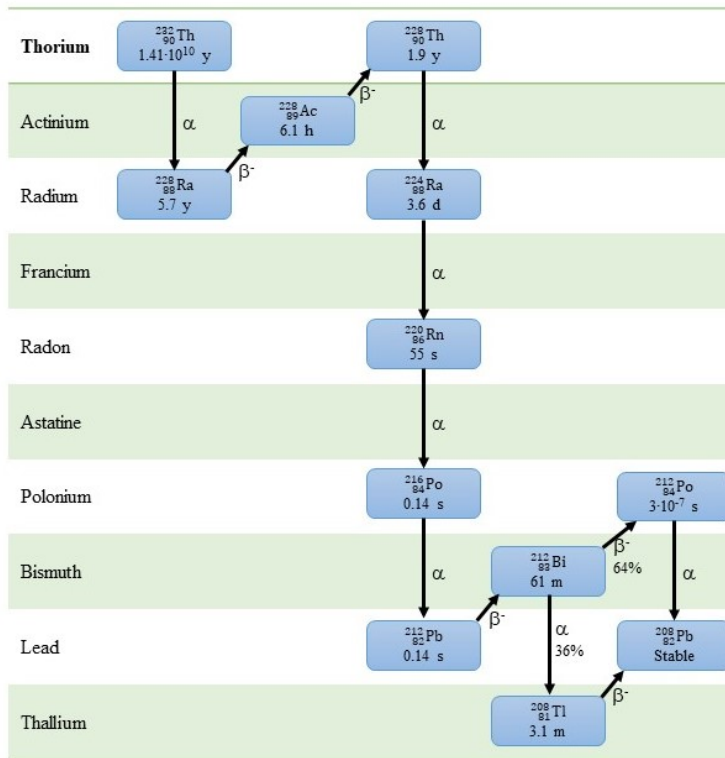
- International Radiation Protection Association (IRPA-10), P-6a-336. 2000.
47. ESS. *Assessment of environmental consequences of the normal operations of ESS facility. Part #1 Input data Source Term. Breakdown of radionuclides & Related basic information.* ESS-0028551. 2016.
 48. Ene, D., Avila, R., Hjerpe, T., Bugay, D., Stenberg, K. *Assessment of environmental consequences of the normal operations of the ESS facility.* Journal of Physics: Conference Series, 1046(1): 012018, 2018.
 49. Ene, D. *Environmental and radiological impacts of the activated air inside the tunnel of ESS accelerator.* ESS-0018010. 2015.
 50. Ene, D. *Source term to the environment from the ESS target station.* Nuclear Energy Agency. NEA/NSC/R(2018)2, p. 32-47. 2018.
 51. Eckerman, K., Harrison, J., Menzel, H., Clement, C. *ICRP publication 119: compendium of dose coefficients based on ICRP publication 60.* Annals of the ICRP, 42(4): e1-e130, 2013.
 52. Valentin, J. *Basic anatomical and physiological data for use in radiological protection: reference values: ICRP Publication 89.* Annals of the ICRP, 32(3-4): 1-277, 2002.
 53. Barkauskas, V., Stenström, K. *Prediction of the radionuclide inventory in the European Spallation Source target using FLUKA.* Nuclear Instruments and Methods in Physics Research Section B: Beam Interactions with Materials and Atoms, 471: 24-32, 2020.
 54. Porstendörfer, J. *Radon: measurements related to dose.* Environment international, 22: 563-583, 1996.
 55. Behbehani, M., Uddin, S., Baskaran, M. *²¹⁰Po concentration in different size fractions of aerosol likely contribution from industrial sources.* Journal of Environmental Radioactivity, 222: 106323, 2020.
 56. Pitz, M., Cyrys, J., Karg, E., Wiedensohler, A., Wichmann, H.-E., Heinrich, J. *Variability of apparent particle density of an urban aerosol.* Environmental Science & Technology, 37(19): 4336-4342, 2003.
 57. Talip, Z., Dressler, R., Schacherl, B., David, J.-C., Vockenhuber, C., Schumann, D. *Radiochemical determination of long-lived radionuclides in proton-irradiated heavy metal targets: Part II Tungsten.* Anal Chem, 93(31): 10798-10806, 2021.
 58. World Health Organization. *Arrangements for preparedness for a nuclear or radiological emergency. Safety guide.* 2007.
 59. ESS. *AA3-Estimations of flow rate and heat transfer.* ESS-0084912. 2018.
 60. Nilsson, P. *Tungsten Oxidation and AeroSol Transport (TOAST).* ESS-0151001. 2018.
 61. Spanier, L. *AA03a_LP-104B Source term to SSM.* ESS-0095522. 2018.
 62. Raj, K. *Effect of WO₃ powder particle shape, size and bulk density, on the grain size and grain size distribution of tungsten metal powder.* Metal Powder Report, 71(4): 285-287, 2016.

Appendix 1.

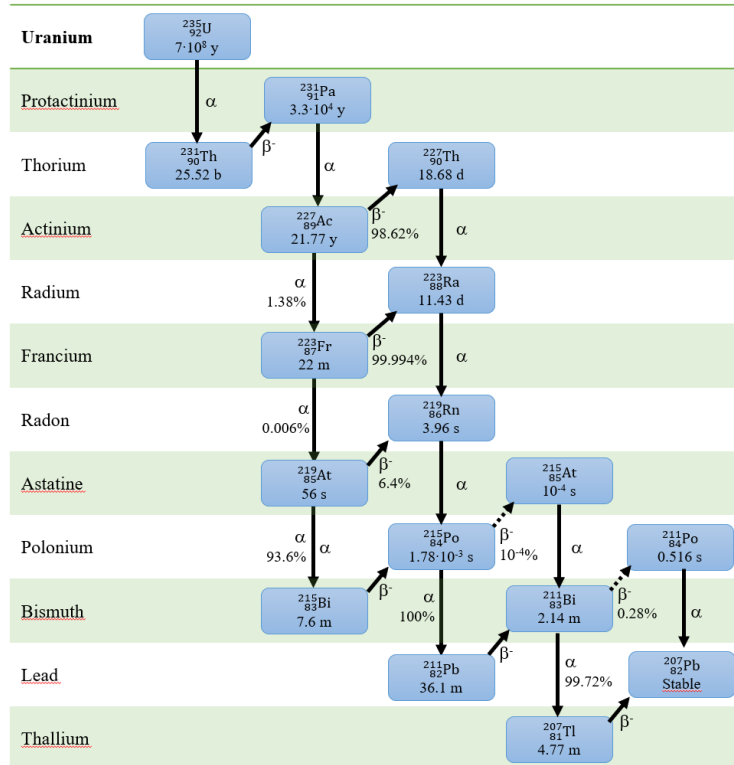
The Uranium Series



The Thorium Series



The Actinium Series



Appendix 2.

Alpha energies for main radionuclides in radon progenies. Branching ratios exceeding 0.1% are included. Data from IAEA Live Chart of Nuclides.

| Series | Nuclide | T _{1/2} | Alpha emission | |
|----------|-------------------|------------------|-------------------------|-------------|
| | | | E _α (keV) | Prob (%) |
| Uranium | ²¹⁸ Po | 3.071 min | 6002.55 | 99.98 |
| Uranium | ²¹⁴ Po | 162.3 μs | 7686.82 | 99.99 |
| Thorium | ²¹² Po | 0.300 μs | 8784.86 | 100 |
| Uranium | ²¹⁰ Po | 138 d | 5304.33 | 100 |
| Thorium | ²¹² Bi | 60.55 min | 5607 | 0.4 |
| | | | 5768 | 0.6 |
| | | | 6050.78 | 25.13 |
| | | | 6089.88 | 9.75 |
| Actinium | ²¹¹ Bi | 2.14 min | 6278.2 | 16.19 |
| | | | 6622.9 | 83.54 |



The Swedish Radiation Safety Authority (SSM) works proactively and preventively with nuclear safety, radiation protection, nuclear security, and nuclear non-proliferation to protect people and the environment from the harmful effects of radiation, now and in the future.

You can download our publications from www.stralsakerhetsmyndigheten.se/en/publications. If you need alternative formats such as easy-to-read, Braille or Daisy, contact us by email at registrator@ssm.se.

Strålsäkerhetsmyndigheten
SE-171 16 Stockholm
+46 (0) 8-799 40 00
www.stralsakerhetsmyndigheten.se
registrator@ssm.se

©Strålsäkerhetsmyndigheten